IOWA STATE UNIVERSITY
Digital Repository

Retrospective Theses and Dissertations

Iowa State University Capstones, Theses and Dissertations

1-1-2003

Robust and fault tolerant flight control design

Dennis Lee Griffin
Iowa State University

Follow this and additional works at: https://lib.dr.iastate.edu/rtd

Recommended Citation

Griffin, Dennis Lee, "Robust and fault tolerant flight control design" (2003). *Retrospective Theses and Dissertations*. 19978.
https://lib.dr.iastate.edu/rtd/19978

This Thesis is brought to you for free and open access by the Iowa State University Capstones, Theses and Dissertations at Iowa State University Digital Repository. It has been accepted for inclusion in Retrospective Theses and Dissertations by an authorized administrator of Iowa State University Digital Repository. For more information, please contact digirep@iastate.edu.

Robust and fault tolerant flight control design

by

Dennis Lee Griffin

A thesis submitted to the graduate faculty

in partial fulfillment of the requirements for the degree of

MASTER OF SCIENCE

Major: Mechanical Engineering

Program of Study Committee:
Atul G. Kelkar, Major Professor
James E. Bernard
Frank R. Chavez

Iowa State University

Ames, Iowa

2003

Copyright © Dennis Lee Griffin, 2003. All rights reserved.

Graduate College
Iowa State University

This is to certify that the master's thesis of

Dennis Lee Griffin

has met the thesis requirements of Iowa State University

Signatures have been redacted for privacy

TABLE OF CONTENTS

LIST OF TABLES v

LIST OF FIGURES vi

ACKNOWLEDGEMENTS ix

1 INTRODUCTION 1

1.1 Literature Review 3

1.2 Contributions of this Work 5

1.3 Thesis Organization 6

2 ROBUST CONTROLLER DESIGN 7

2.1 Introduction 7

2.2 Mathematical Model 8

2.3 Controller Design 11

2.3.1 LQG Design 11

2.3.2 McFarlane-Glover Robustification 16

2.3.3 H_∞ Controller Design 32

2.4 Comparison of Controller Designs 38

2.5 Remarks 40

3 AIRCRAFT FAULT DESCRIPTION 44

3.1 Introduction 44

3.2 Aircraft Model and Fault Description 45

3.2.1 Lock-In-Place Actuator Fault 46

3.3 Fault Model for Fighter Aircraft Configuration 47
3.4 Effect on System Response 49
3.5 Summary Remarks 54

4 FAULT TOLERANT CONTROLLER FORMULATION 56

4.1 Introduction 56
4.2 Problem Formulation 57
4.3 Controller Formulation 57
4.4 Simulation 60
4.5 Comparison of Robust H_∞ and Adaptive Methods 64
4.5.1 Mathematical model 64
4.5.2 Simulation 66
4.5.3 Regulation 70
4.5.4 Tracking 71
4.6 Conclusions 74

5 CONCLUSIONS AND FUTURE WORK 81

5.1 Concluding Remarks 81
5.1.1 Suggestions for Future Work 82

BIBLIOGRAPHY 84

LIST OF TABLES

Table 2.1 Open-loop eigenvalues 10

Table 2.2 LQG closed-loop eigenvalues 15

Table 2.3 Closed-loop eigenvalues with McFarlane-Glover design 29

Table 3.1 Response to control surface deflection 45

Table 3.2 LQR stability comparison 49

Table 3.3 LQG stability comparison 50

Table 3.4 McFarlane Glover stability comparison 50

Table 3.5 H_∞ stability comparison 51

Table 4.1 Eigenvalues of Boeing 747 lateral dynamics 66

LIST OF FIGURES

Figure 2.1 Schematic of fighter aircraft model 8

Figure 2.2 Open-loop singular values 11

Figure 2.3 LQG closed loop system 13

Figure 2.4 LQG controller singular values 15

Figure 2.5 LQG pitch response 16

Figure 2.6 LQG angle of attack response 17

Figure 2.7 LQG roll attitude response 18

Figure 2.8 LQG roll response 19

Figure 2.9 LQG normal load factor response 20

Figure 2.10 LQG lateral load response 21

Figure 2.11 LQG yaw response 22

Figure 2.12 Feedback system for robustified design 22

Figure 2.13 McFarlane-Glover controller singular values 28

Figure 2.14 McFarlane-Glover pitch response 29

Figure 2.15 McFarlane-Glover angle of attack response 30

Figure 2.16 McFarlane-Glover roll attitude response 30

Figure 2.17 LQG roll response 31

Figure 2.18 McFarlane-Glover normal load factor response 31

Figure 2.19 McFarlane-Glover lateral load response 32

Figure 2.20 McFarlane-Glover yaw response 32

Figure 2.21 Relative uncertainty 33

Figure 2.22 Multiplicative uncertainty weight 34
Figure 2.23 System with multiplicative uncertainty weight 34
Figure 2.24 Sensitivity Weighting Function 36
Figure 2.25 Generalized plant for the stacked problem 36
Figure 2.26 H_∞ Controller singular values 37
Figure 2.27 H_∞ pitch response 38
Figure 2.28 H_∞ angle of attack response 39
Figure 2.29 H_∞ roll attitude response 40
Figure 2.30 H_∞ roll response 41
Figure 2.31 H_∞ normal load factor response 41
Figure 2.32 H_∞ lateral load response 42
Figure 2.33 H_∞ yaw response 42
Figure 2.34 Maximum singular value of the closed-loop system 43
Figure 2.35 Maximum singular value of sensitivity function 43

Figure 3.1 Failure comparison (pitch response) 51
Figure 3.2 Failure comparison (normal load response) 52
Figure 3.3 Failure comparison (angle of attack response) 52
Figure 3.4 Failure comparison (yaw rate response) 53
Figure 3.5 Failure comparison (roll rate response) 53
Figure 3.6 Failure comparison (lateral load response) 54
Figure 3.7 Failure comparison (roll attitude response) 54

Figure 4.1 Nominal closed loop system 58
Figure 4.2 Standard block diagram form 58
Figure 4.3 Closed loop system with failure Uncertainty 59
Figure 4.4 General plant configuration 60
Figure 4.5 Performance weight bode plot 62

Figure 4.6 Controller singular values 64
Figure 4.7 Maximum sensitivity singular values 65
Figure 4.8 Pitch rate response (H_∞) 66
Figure 4.9 Normal load response (H_∞) 67
Figure 4.10 Angle of attack response (H_∞) 68
Figure 4.11 Yaw rate response (H_∞) 69
Figure 4.12 Roll rate response (H_∞) 70
Figure 4.13 Lateral load response (H_∞) 71
Figure 4.14 Roll attitude response (H_∞) 72
Figure 4.15 Performance weight bode plot 73
Figure 4.16 Controller singular values 74
Figure 4.17 Maximum sensitivity singular values 75
Figure 4.18 Side slip angle response 75
Figure 4.19 Yaw rate response 76
Figure 4.20 Roll rate response 76
Figure 4.21 Roll angle response 77
Figure 4.22 Side slip angle tacking response 77
Figure 4.23 Yaw rate tracking response 78
Figure 4.24 Roll rate tracking response 78
Figure 4.25 Roll angle tracking response 79
Figure 4.26 Adaptive controller inputs 79
Figure 4.27 H_∞ controller inputs 80

ACKNOWLEDGEMENTS

I am extremely grateful for the time, support, and knowledge given by Dr. Atul Kelkar throughout my academic career and throughout this project. I also want to thank Dr. James Bernard and Dr. Frank Chavez for their inspiration and help in serving on my program of study committee. Special thanks goes to my entire family, especially my parents, who have all supported me throughout my academic career and encouraged me to pursue my interests. I would like to dedicate this paper to Erin; for her love, support, and patience helped make this possible. Finally, I would like to acknowledge the financial support from NASA through the Iowa Space Grant Consortium and from NSF through grant Nos. CMS 0196198 and CMS 0196391.

1 INTRODUCTION

Over the past several years, methods for reliable and reconfigurable fault tolerant control of aircraft have been researched extensively. The motivation for this development is that many existing control systems on aircraft will not guarantee dynamic stability in the presence of one or more control surface failures due to the subsequent performance degradation of the control system. The deterioration inherited by the aircraft may then cause the pilot to lose control of the aircraft. In case of such a failure there is a potential loss of hundreds of human lives coupled with millions of dollars to replace the aircraft. Furthermore, due to proposed safety regulations by the Federal Aviation Administration FAA and similar military interests, the need for aircraft that can withstand control surface failures is greatly increasing. For example, the FAA performance target for commercial aircraft is, by 2007, to reduce the airline fatal accident rate by 80% from the 1994-1996 baseline and continue to maintain the low rate from then on. In order to meet these needs the aircraft control systems must be designed to accomodate potential actuator and sensor failures while maintaining overall stability and reasonable performance. This requirement translates to the control objective of maintaining adequate stability and performance during all flight conditions including the period after a loss or break down of a control surface. Recent incidents of aircraft Loss of Control (LOC) caused by control surface failures are given below to illustrate the need for fault tolerant control systems.

1. On June 4, 2003 at Seymour Johnson air force base in Utah the pilot of a F-15E

Strike Eagle lost control of the aircraft after a shaft connected to the pilots controls disconnected from the right stabilizer causing a complete loss of effectiveness of that control surface. The pilot and co-pilot onboard ejected and survived, but the $40.4 million aircraft was destroyed.

2. In another incident, in 1989, a DC-10 aircraft executed an emergency crash landing in Sioux City, IA, after its hydraulic system was totally disabled by shrapnel from the failure of its tail engine. The pilots managed to crash land the plane using only wing engine thrust.

These examples indicate that the failure of actuators and/or sensors on board of aircraft is always a possibility.

Most civil transport aircraft and military aircraft use eight separate control surfaces to achieve desired flight performance. Any one of these can fail for reasons such as hydraulic system failure, ice build-up on the wings and tail, or a failed connection from the control system computer to the control surface actuators. These failures and others can all be classified into one of the following types: Lock-In-Place (LIP); Hard-Over-Failure (HOF); Float; and Loss of Effectiveness (LOE) all of which may have disastrous effects. However, many of the control surfaces are redundant in the sense that they can produce similar dynamics, leaving the aircraft with the ability to be stabilized with proper reconfiguration of the control surfaces. The goal of the reliable or reconfigurable fault tolerant control system is then to assure stability in the aircraft, even with control surface failures, by taking advantage of the redundancy in the control surfaces. Several methods have been used to accomplish this including adaptive techniques, model predictive techniques, switching and tuning techniques, and H_∞ techniques.

The H_∞ design techniques have been utilized since the beginning of the 1980's to design controllers that are robust to plant uncertainties. In the case of the mixed sensitivity problem, the uncertainty is usually expressed by the designer by forming weighting func-

tions to impose conditions on certain signals in the system which are known to contain some uncertainty. The McFarlane - Glover robustification method, however, attempts to maximize the amount of coprime-uncertainty the system can withstand and does not require the use of weighting functions. Several control design methods have been developed for designing robust controllers for systems wherein the plant uncertainty description is given in terms of parametric uncertainty and/or measurement uncertainty caused by outside disturbances. However, little work has been done on the modelling and control of systems with control surface failure types of uncertainties. In particular, applications of H_∞ controller design in this area have not been thoroughly investigated.

The difference between the H_∞ controller approach and the more common fault accommodation techniques is that only a single controller is used to stabilize the system. In most methods the use of controller switching is required in the event of failure. The attraction of using a single controller design to account for system faults is that there are no switching transients that may de-stabilize the system during a fault and there is no need for complicated fault detection systems. Fault detection and isolation (FDI) systems have problems in that false fault detections may occur and the control system may inadvertently de-stabilize the aircraft. Also there are delays required to both detect and isolate the fault.

The goal of the research presented in this thesis is to eliminate the problems encountered by FDI systems by focusing on the development of reliable control techniques that can robustify the control system and account for control surface failures.

1.1 Literature Review

A considerable amount of research has been done on the topic of reconfigurable fault tolerant flight control techniques within the last decade. Most of the current methods utilize a control system in which multiple controllers are predesigned - one for the nominal

"healthy" system and one for each of the possible fault scenarios. One such technique is multi-mode switching control which uses Model Predictive Control (MPC) and Multiple Models, Switching and Tuning (MMST) techniques. This method uses observers which detect the type of failure that has occurred by measuring the dynamics of the aircraft and estimating the input to the aircraft. The system can then switch to the appropriate controller in order to stabilize the aircraft. Another method uses an adaptive algorithm technique to continuously update controller parameters to stabilize the aircraft at the inset of a fault. Although there is a large collection of literature on the use of switching control techniques, there is limited literature on the use of a single controller design which is robust to a set of fault scenarios and still provides adequate performance. The effective single controller designs that have been presented in literature are mostly based on H_∞ control methods. A brief review of H_∞ control theory is presented next as a background for control design development presented later.

Robust control methods that can solve H_∞ based control problems have existed since the early 1980's. The original H_∞ control theory was first introduced by Zames [1981]. This theory was the first to look at bringing plant uncertainty, specified in the frequency domain, into use in modern control techniques. Soon after Doyle [1984] presented the first solution to a general rational multi-input multi-output H_∞ optimal control problem. This procedure involved co-prime factorizations of transfer function matrices that reduced the problem to a Hankel norm problem. This problem was then solvable by the state-space methods presented by Glover [1984]. Similar approaches were also presented in [Francis and Doyle, 1987]. However, these first methods that were developed produced very high controller orders and were difficult to work with. More recent advances include Doyle's paper on State-space solutions to standard H_2 and H_∞ control problems [1989] and Glover and McFarlane's paper on robust H_∞ stabilization of normalized co-prime factor plant descriptions [1989]. These methods produced controllers comparable to the original plant order. As the development of the personal computer grew these methods

began to be used more in applications as larger and more complex systems were introduced and the use of more classical control methods, such as Bode's gain and phase margin techniques became impractical. Also, these methods provide a very good means of accounting for various uncertainties in a system such as parametric uncertainties in the actual plant, uncertainties in the control input signal, and uncertainties in the signal measurements from the output of the system. In short, the use of H_∞ techniques for the use of controller design has rapidly advanced over the past decade and has been shown to work for a wide range of problems.

Robust H_∞ control methods have just recently been used in the problem of fault tolerant flight control. As expected, for fault tolerant control problems the uncertainty in the system is the set of possible fault scenarios that may possibly occur. One paper that has looked at this method is Komatsu's paper on the realization of fault tolerant control for the reusable launch vehicle [2002]. This paper presents an H_∞ controller design method by using an input multiplicative uncertainty weight to model the fault uncertainty. Furthermore, it is shown that the method is successful in stabilizing the launch vehicle in the presence of Loss of Effectiveness actuator faults. Another paper, written by Jonckheere presents a method of H_∞ control using model matching techniques. This paper also shows that the concept is workable for various aircraft models.

1.2 Contributions of this Work

This thesis is aimed at two specific research objectives:

1. The first objective is to explore three different control design methodologies, namely, LQG, H_∞, and McFarlane-Glover robustifying technique for the design of an aircraft autopilot for a civilian as well as a fighter aircraft system.

   For this work, it is assumed that the aircraft is "healthy", i.e., it has all the control surfaces and sensors working properly. All three controller designs are compared

via simulated time and frequency responses and some conclusions are made.

2. The second objective is to explore the feasibility of modeling the actuator surface failures as some kind of plant uncertainty and design a single robust controller that can accommodate failure types of uncertainty while maintaining closed-loop stability with acceptable level of performance.

   For this work, a particular type of failure considered is the Lock-In-Place (LOP) actuator (control surface) failure. The two advanced control designs evaluated include McFarlane-Glover robustifying design and a mixed sensitivity H_∞ design. The McFarlane - Glover technique is used on a baseline LQG controlled system Furthermore, this design methodology is shown to be applicable to a civilian as well as military type of aircraft which have significantly different dynamics. This control method also sets a foundation for the development of a similar H_∞-based fault tolerant control strategy.

1.3 Thesis Organization

The organization of this thesis is as follows: Chapter 2 presents a mathematical model of an aircraft which is chosen as the focus configuration for comparing different robust controller designs for an autopilot. The uncertainties considered are in the parameters of the phugoid modes of the system. Numerous simulation results are given to present time as well as frequency responses to compare three different controllers. Chapter 3 describes various actuator faults that commonly occur and then develops the framework for describing the "faulty" plant. This plant model is then used for the design of fault tolerant control system. In particular, the actuator failure considered is that of locked ailerons and rudder. Chapter 4 presents the results for fault tolerant control design for a jet fighter aircraft model as well as a civil transport aircraft model. Finally, Chapter 5 gives some concluding remarks and suggestions for future work.

2 ROBUST CONTROLLER DESIGN

2.1 Introduction

In spite of considerable amount of literature [23, 1, 43, 2, 21, 24, 26, 37, 38] that exists on the design of automatic flight control systems, the research effort in this area continues to grow as a result of continued advances made in the areas of control theory, actuator/sensor technology, propulsion technology, and materials technology. In the light of these technological advances numerous new possibilities exist for improving the existing autopilot designs. In particular, the robust control design methodologies emerged during last decade [22, 36, 6, 13, 18, 21, 30, 44, 45] have had tremendous impact on the control design methodologies. Specifically, in the applications such as flight control where human lives are at stake it becomes extremely important to ensure that autopilot design is made as robustly stable as possible especially for civil transport aircraft. This research is aimed at evaluating different robust control strategies for an aircraft autopilot design. The objective of the control design is not only the stability robustness and performance under normal operating conditions but also in the presence of actuator failures. Different control paradigms considered include LQG, H_∞, and McFarlane Glover-based robustified control design. This chapter focuses on presenting underlying mathematical framework for these controller designs and developing mathematical model of the aircraft system which is the target application.

2.2 Mathematical Model

Two robust control design methodologies are evaluated using a multi-input multi-output (MIMO) aircraft autopilot configuration using an example of a fighter aircraft model shown in Fig. 2.1 (taken from [23]). A linearized dynamic model of the fighter

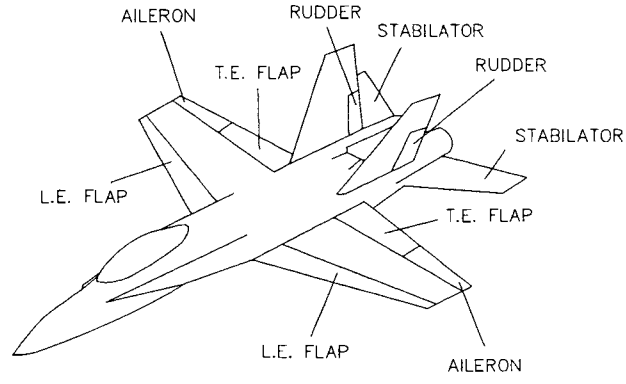

Figure 2.1 Schematic of fighter aircraft model

aircraft configuration shown in Fig. 2.1 is given in the state-space form as follows:

$$\begin{aligned} \dot{x}(t) &= Ax(t) + Bu(t) \\ y(t) &= Cx(t) + Du(t) \end{aligned} \tag{2.1}$$

where, the state variable vector $x(t)$ is given by

$$x(t) = \left[\; u(t), \;\; w(t), \;\; q(t), \;\; \theta(t), \;\; v(t), \;\; p(t), \;\; r(t), \;\; \phi(t) \; \right]^T$$

The state variables represent change in forward velocity (u), change in vertical velocity (w), change in pitch rate (q), change in pitch attitude (θ), change in sideslip velocity (v), change in rolling velocity (p), change in yawing velocity (r), and change in rolling attitude (ϕ).

The control input vector u is given by

$$u(t) = \left[\; \delta_{SSYM}(t), \;\; \delta_{LEF}(t), \;\; \delta_{TEF}(t), \;\; \delta_{SDIFF}(t), \;\; \delta_{LEFD}(t), \;\; \delta_{TEFD}(t), \;\; \delta_A(t), \;\; \delta_R(t) \; \right]^T$$

where, δ_{sSYM}, δ_{LEF}, and δ_{TEF} denote the inputs due to longitudinal control surfaces, symmetrical stabilizer, leading edge flaps, and trailing edge flaps, respectively. The control inputs δ_{SDIFF}, δ_{LEFD}, δ_{TEFD}, δ_A, and δ_R are for the lateral motion caused by differential stabilizer, differential leading edge flap, differential trailing edge flap, aileron, and rudder, respectively. The output vector y is given by

$$y = \begin{bmatrix} q & n_{zcg} & \alpha & r & p & n_{ycg} & \phi \end{bmatrix}^T$$

which represent the pitch rate, normal acceleration at the C.G., angle of attack, yaw rate, roll rate, lateral acceleration at the C.G., and roll attitude. The system matrices A, B, C, and D (taken from [23]) at the flight condition of Mach 0.6 and at the altitude of 3000 meters are given by

$$A = \begin{bmatrix} -.0133 & -.0173 & -29.2 & -32.2 & 0 & 0 & 0 & 0 \\ -.073 & -1.14 & 636.0 & -1.46 & 0 & 0 & 0 & 0 \\ .000012 & -.011 & -.81 & .0005 & 0 & 0 & 0 & 0 \\ 0 & 0 & 1.0 & 0 & 0 & 0 & 0 & 0 \\ 0 & 0 & 0 & 0 & -.244 & -645 & 29.5 & 32.2 \\ 0 & 0 & 0 & 0 & .007 & -.217 & -.015 & 0 \\ 0 & 0 & 0 & 0 & -.029 & .7 & -3.12 & 0 \\ 0 & 0 & 0 & 0 & 0 & .046 & 1.0 & 0 \end{bmatrix}$$

$$B = \begin{bmatrix} 0 & 0 & 0 & 0 & 0 & 0 & 0 & 0 \\ -.2 & -.645 & -.456 & 0 & 0 & 0 & 0 & 0 \\ -.241 & -.523 & .328 & 0 & 0 & 0 & 0 & 0 \\ 0 & 0 & 0 & 0 & 0 & 0 & 0 & 0 \\ 0 & 0 & 0 & -.21 & 0 & 0 & 0 & 30.37 \\ 0 & 0 & 0 & .574 & 0 & -.327 & .0044 & -.465 \\ 0 & 0 & 0 & .395 & 0 & 2.49 & 25.2 & 41.3 \\ 0 & 0 & 0 & 0 & 0 & 0 & 0 & 0 \end{bmatrix}$$

$$C = \begin{bmatrix} 0 & 0 & 1.0 & 0 & 0 & 0 & 0 & 0 \\ -.0023 & -.0354 & -.324 & -.0453 & 0 & 0 & 0 & 0 \\ 0 & .0016 & 0 & 0 & 0 & 0 & 0 & 0 \\ 0 & 0 & 0 & 0 & 0 & 1.0 & 0 & 0 \\ 0 & 0 & 0 & 0 & 0 & 0 & 1.0 & 0 \\ 0 & 0 & 0 & 0 & -.0076 & .044 & .9162 & 0 \\ 0 & 0 & 0 & 0 & 0 & 0 & 0 & 1.0 \end{bmatrix}$$

$$D = \begin{bmatrix} 0 & 0 & 0 & 0 & 0 & 0 & 0 & 0 \\ -.0062 & .021 & -.014 & 0 & 0 & 0 & 0 & 0 \\ 0 & 0 & 0 & 0 & 0 & 0 & 0 & 0 \\ 0 & 0 & 0 & 0 & 0 & 0 & 0 & 0 \\ 0 & 0 & 0 & 0 & 0 & 0 & 0 & 0 \\ 0 & 0 & 0 & -.00065 & 0 & 0 & 0 & .943 \\ 0 & 0 & 0 & 0 & 0 & 0 & 0 & 0 \end{bmatrix}$$

The open-loop eigenvalues of the system which were calculated are given in Table 2.1.

Mode	Eigenvalue	Frequency (rad/s)	Damping ratio
Phugoid	$-0.007 \pm j0.057$	0.057	0.122
Short Period	$-0.98 \pm j2.63$	2.810	0.349
Spiral	-0.001	0.001	1.000
Roll Subsidence	-3.01	3.010	1.000
Dutch Roll	$-0.286 \pm j2.25$	2.270	0.126

Table 2.1 Open-loop eigenvalues

The open-loop singular values of the system are shown in Fig. 2.2.

The objective is to design an autopilot that is robust to parametric and modelling uncertainties and can achieve a desirable performance. It is also desired to obtain a

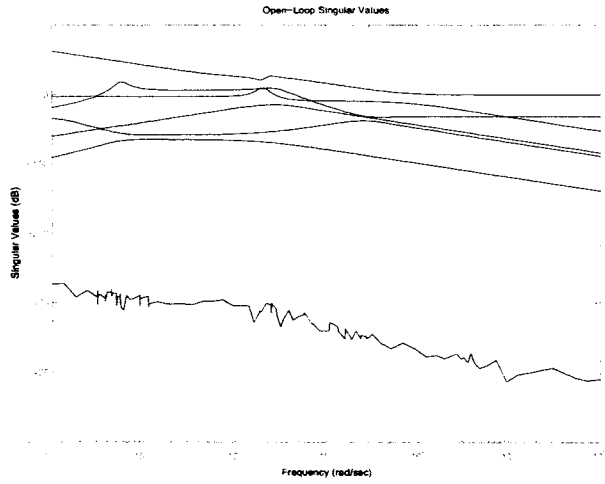

Figure 2.2 Open-loop singular values

quantitative assessment of robustness achieved by the controller in terms of the percentage of uncertainty that can be tolerated. The next section gives details of the design procedure used to obtain a robust controller that achieves these objectives.

2.3 Controller Design

This section will focus on various controller designs. In particular, the design methodologies considered include LQG, McFarlane-Glover-based two-loop design, and an H_∞ design. The first three subsections will present each of these designs and then the subsequent section will present a comparison of these three designs.

2.3.1 LQG Design

Let the aircraft system under consideration be described by the following set of equations:

$$\dot{x}(t) = Ax(t) + Bu(t) + \eta(t)$$

$$m(t) = Cx(t) + Du(t) + \zeta(t) \tag{2.2}$$

$$y(t) = m(t)$$

where $u(t)$ is the control input, $\eta(t)$ is the actuator noise, $\zeta(t)$ is the measurement noise, $y(t)$ is the performance output, and $m(t)$ is the measurement output. $\eta(t)$ and $\zeta(t)$ are assumed to be uncorrelated zero mean white noise processes. The performance function for LQG was considered as:

$$J = E\left\{\frac{1}{2}\int_0^\infty \left[x(t)^T Q x(t) + u^T(t) R u(t)\right] dt\right\} \tag{2.3}$$

where matrices $Q = Q^T \geq 0$ and $R = R^T > 0$ denote the state and control weighting, respectively. The state weighting matrix Q is selected to be $Q = C^T \hat{Q} C$ where $\hat{Q} = \hat{Q}^T \geq 0$ is the design parameter. This selection of Q allows weighting of outputs instead of a complete state vector.

The optimal control input is given by:

$$u(t) = -K\hat{x}(t) = -R^{-1}B^T P\hat{x}(t) \tag{2.4}$$

where, $\hat{x}(t)$ is the estimated state, K is the regulator gain, and P is the solution of the following (steady-state) algebraic Riccati equation (ARE):

$$A^T P + PA - PBR^{-1}B^T P + Q = 0 \tag{2.5}$$

$\hat{x}(t)$ is the solution of following observer (Kalman filter) dynamics:

$$\dot{\hat{x}}(t) = (A - LC - BK)\hat{x}(t) + LCx(t) + L\zeta(t) \tag{2.6}$$

where, L is the Kalman gain given by: $L = \Sigma(t)C^T V^{-1}$. $V = E\left[\zeta\zeta^T\right]$ and Σ is the solution of the following ARE called as the filter Riccati equation.

$$\Sigma A^T + A\Sigma - \Sigma C^T V^{-1} C\Sigma + BW^{-1}B^T = 0 \tag{2.7}$$

where, $W = E\left[\eta\eta^T\right]$.

The LQG controller is the combination of the Kalman filter (Eq. 2.6) and regulator (Eq. 2.4).

The closed-loop system is given by

$$\begin{aligned}
\begin{bmatrix} \dot{x}(t) \\ \dot{\hat{x}}(t) \end{bmatrix} &= \begin{bmatrix} A & -BK \\ LC & A - LC - BK + LDK \end{bmatrix} \begin{bmatrix} x(t) \\ \hat{x}(t) \end{bmatrix} \\
&+ \begin{bmatrix} \eta(t) \\ L\zeta(t) \end{bmatrix} \\
y &= \begin{bmatrix} C & -DK \end{bmatrix} \begin{bmatrix} x(t) \\ \hat{x}(t) \end{bmatrix} + \zeta(t)
\end{aligned} \tag{2.8}$$

A block diagram of the feedback control system is given in Fig. (2.3).

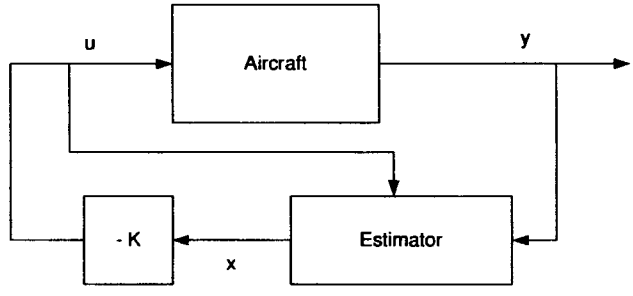

Figure 2.3 LQG closed loop system

The control design parameters were chosen as, Q and R are taken from [23]:

$$\begin{aligned}
\hat{Q} &= \text{diag}\,[200,\ 7,\ 7,\ 10,\ 1,\ 6,\ 1] \\
R &= \text{diag}\,[1,\ 100,\ 50,\ 1,\ 100,\ 60,\ 5,\ 10]
\end{aligned}$$

$$W = 10^4 \times \text{diag}\left[10^6,\ 10^6,\ 10^6,\ 1,\ 1,\ 1,\ 1,\ 1\right]$$
$$V = I_7 \tag{2.9}$$

For these design parameters, the state feedback gain matrix and the observer gain are calculated as

$$K = \begin{bmatrix} -0.003 & -0.028 & -15.606 & -1.900 & 0 & 0 & 0 & 0 \\ -0.000 & -0.001 & -0.340 & -0.041 & 0 & 0 & 0 & 0 \\ .000 & .001 & 0.424 & 0.054 & 0 & 0 & 0 & 0 \\ 0 & 0 & 0 & 0 & -0.004 & 3.926 & 0.039 & -0.744 \\ 0 & 0 & 0 & 0 & 0 & 0 & 0 & 0 \\ 0 & 0 & 0 & 0 & 0 & -0.037 & 0.003 & 0.009 \\ 0 & 0 & 0 & 0 & -0.002 & .077 & .411 & 0.242 \\ 0 & 0 & 0 & 0 & -0.004 & -0.0166 & 0.557 & 0.181 \end{bmatrix}$$

$$L = 10^6 \times \begin{bmatrix} -0.09379 & -3.0551 & -2.323 & 0 & 0 & 0 & 0 \\ -0.0168 & -0.0570 & 0.0802 & 0 & 0 & 0 & 0 \\ 0.0956 & -0.0293 & 0 & 0 & 0 & 0 & 0 \\ 0.0240 & 0.0783 & 0.0575 & 0 & 0 & 0 & 0 \\ 0 & 0 & 0 & 0.0026 & 0.0672 & -0.0739 & 0 \\ 0 & 0 & 0 & 0.0999 & -0.0012 & 0.0032 & 0 \\ 0 & 0 & 0 & -0.0012 & 0.0740 & 0.0672 & 0 \\ 0 & 0 & 0 & 0 & 0 & 0 & 0.1 \end{bmatrix}$$

The resulting singular values of the LQG controller are shown in Fig. (2.4).

The closed-loop eigenvalues are listed in Table (2.2).

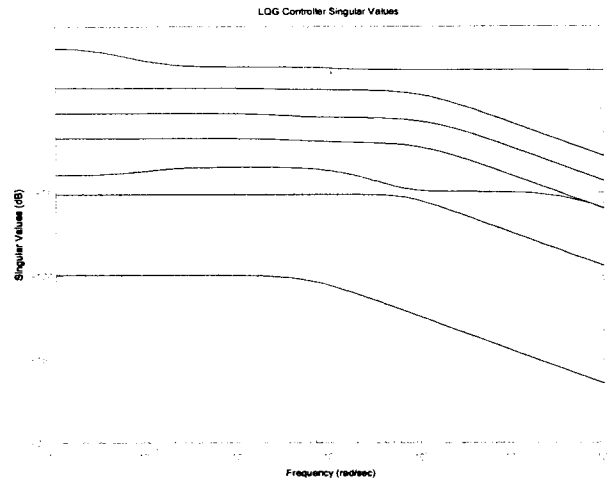

Figure 2.4 LQG controller singular values

Mode	Eigenvalue	Frequency (rad/s)	Damping ratio
Phugoid	$-0.021 \pm j0.032$	0.0387	0.55
Short Period	$-3.000 \pm j2.916$	4.190	0.717
Spiral	-0.612	0.612	1.000
Roll Subsidence	-36.23	36.23	1.000
Dutch Roll	$-1.176 \pm j1.931$	2.260	0.520

Table 2.2 LQG closed-loop eigenvalues

The open-loop and closed-loop responses for the LQG controlled system to an initial angle of attack of, $\alpha = 0.0015$ rad and to an initial sideslip velocity disturbance of 6.5 ft/s are given in Figs. 2.5 through 2.11. These responses show a desirable improvement from the uncontrolled system response. Having obtained the baseline LQG design that gives desirable performance, an outer-loop robustifying controller is designed next as given in section 3.2. The outer-loop will be designed to make this LQG design tolerant to some level of plant uncertainties which traditional LQG designs are not.

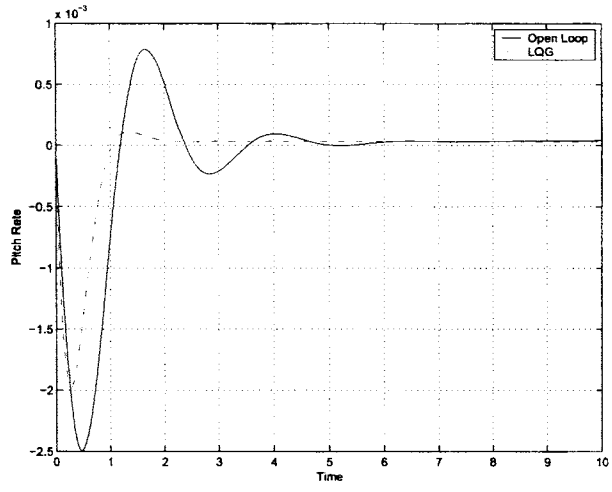

Figure 2.5 LQG pitch response

2.3.2 McFarlane-Glover Robustification

The McFarlane-Glover loop shaping technique, originally introduced in 1990, consists of pre-and-post-compensation of the plant. This controller design methodology is a two-step process. The first step involves design of an inner-loop controller whose primary objective is to achieve the best possible performance (i.e., shape the plant to meet high performance levels) without any consideration to stability robustness. Then, in the second step of the design, the focus is on obtaining an outer-loop controller that robustifies the overall design (i.e., provides increased stability margins) using the McFarlane-Glover H_∞ loop shaping procedure. In this work, an LQG-based design is used as the baseline design or hereafter referred to as the inner-loop design. In the second step, the compensated plant is robustified with respect to coprime uncertainty using an H_∞-optimal loop shaping technique (suggested by McFarlane-Glover [22]).

The classical control design techniques typically lack guarantees of robust stability especially for MIMO systems since there is no systematic way to handle simultaneous perturbations possibly occurring in different loops. It is now a common practice to

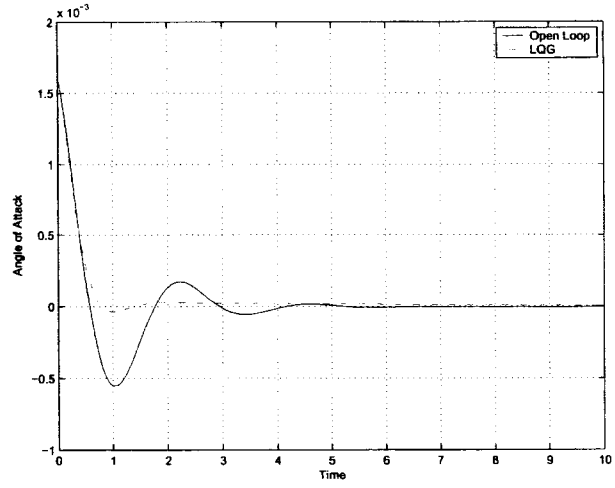

Figure 2.6 LQG angle of attack response

model such perturbations using norm-bounded dynamic matrix perturbations. This allows controls engineers to quantify the robustness levels by examining the maximum singular values of appropriate closed-loop transfer functions. Given below is a brief theoretical background to the robust stabilization procedure.

Consider a plant with normalized left coprime factorization

$$G = M^{-1}N \tag{2.10}$$

Let the plant model in Eq. (2.10) have some uncertainties and let the perturbed plant be modelled as

$$G_p = (M + \Delta_M)^{-1}(N + \Delta_N) \tag{2.11}$$

where, Δ_M and Δ_N are stable unknown transfer functions representing uncertainty in the plant. Then, the robust control problem at hand is to design a feedback controller to stabilize a family of the perturbed plants given by

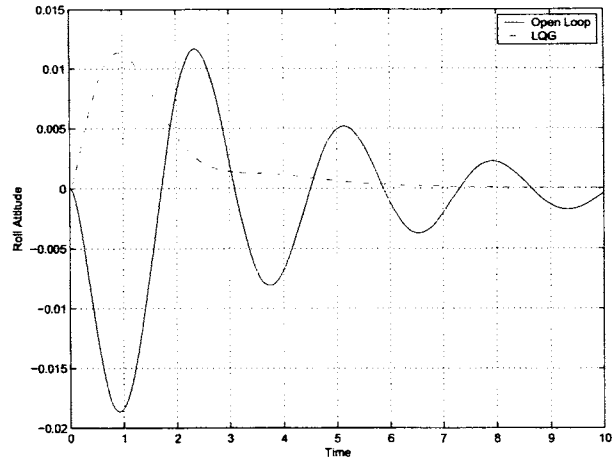

Figure 2.7 LQG roll attitude response

$$G_p = \{(M + \Delta_M)^{-1}(N + \Delta_N) : \| \begin{bmatrix} \Delta_N & \Delta_M \end{bmatrix} \|_\infty < \varepsilon\} \tag{2.12}$$

where $\varepsilon > 0$ gives the stability margin. The McFarlane-Glover solution to this robust stabilization problem is to maximize the stability margins. The feedback system of Fig.2.12 is robustly stable if and only if the nominal feedback system is stable and the following condition is satisfied.

$$\gamma \triangleq \left\| \begin{bmatrix} K \\ I \end{bmatrix} (I - GK)^{-1} M^{-1} \right\|_\infty \leq \frac{1}{\varepsilon} \tag{2.13}$$

The minimum achievable γ and the corresponding stability margin is given by

$$\gamma_{min} = \varepsilon_{max}^{-1} = \left\{1 - \| \begin{bmatrix} N & M \end{bmatrix} \|_H^2\right\}^{\frac{-1}{2}} = (1 + \rho(XZ))^{\frac{1}{2}} \tag{2.14}$$

where, $\| \cdot \|_H$ denotes the Hankel norm, ρ is the spectral radius, and $Z > 0$ is the unique solution to the following ARE

$$(A - BS^{-1}D^TC)Z + Z(A - BS^{-1}D^TC)^T -$$

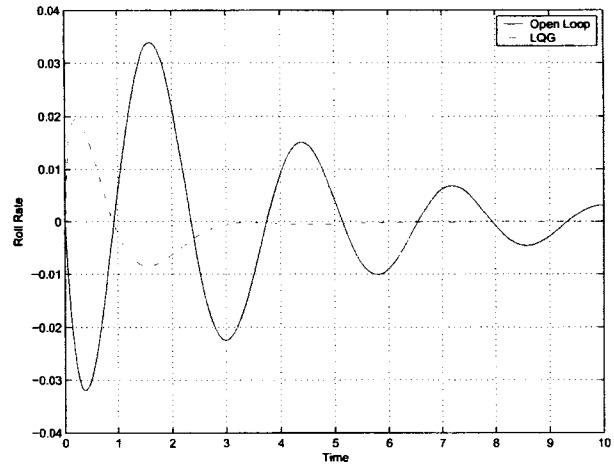

Figure 2.8 LQG roll response

$$ZC^T R^{-1} CZ + BS^{-1} B^T = 0 \tag{2.15}$$

where, $(A,\ B,\ C,\ D)$ is the minimal realization and

$$R = I + DD^T$$

$$S = I + D^T D$$

Similarly, $X > 0$ is the unique solution to the following ARE

$$(A - BS^{-1} D^T C)^T X + X(A - BS^{-1} D^T C) - XBS^{-1} B^T X + C^T R^{-1} C = 0 \tag{2.16}$$

The controller that guarantees the inequality

$$\left\| \begin{bmatrix} K \\ I \end{bmatrix} (I - GK)^{-1} M^{-1} \right\|_\infty \leq \gamma$$

is given by the following closed-form expressions for a given $\gamma > \gamma_{min}$:

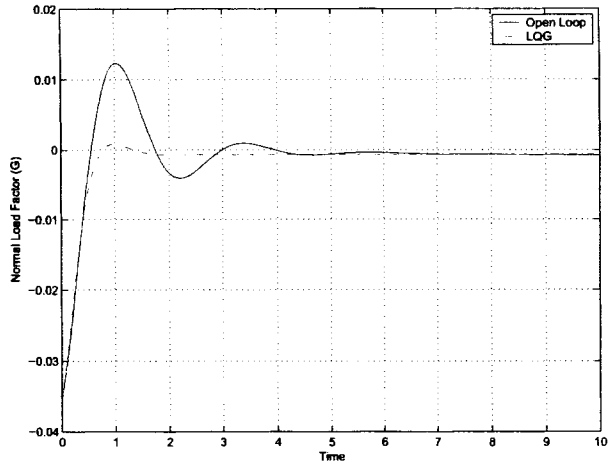

Figure 2.9 LQG normal load factor response

$$K \stackrel{s}{=} \left[\begin{array}{c|c} A+BF+\gamma^2(L^T)^{-1}ZC^T(C+DF) & \gamma^2(L^T)^{-1}ZC^T \\ \hline B^TX & -D^T \end{array}\right]$$

where,

$$F = -S^{-1}(D^TC + B^TX)$$

$$L = (1-\gamma^2)I + XZ$$

The most attractive feature of McFarlane-Glover technique lies in the fact that one can use the control design technique of one's choice to achieve the best possible performance without any considerations to uncertainties in the plant and then use the McFarlane-Glover procedure to enhance robustness (i.e., "robustify") in the outer-loop by sacrificing performance only to the extent necessary. Moreover, this procedure allows to quantify the level of robustness that one has achieved in the process. A numerical example given in section 4.0 will illustrate this design and compare with LQG and H_∞ designs, as well.

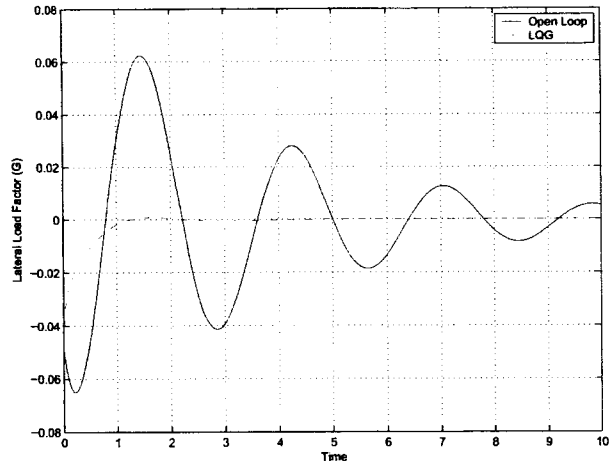

Figure 2.10 LQG lateral load response

The McFarlane-Glover design resulted in the following controller parameters:

$$S = \begin{bmatrix} 1.0000 & -.0001 & .0001 & 0 & 0 & 0 & 0 & 0 \\ -.0001 & 1.0004 & -.0003 & 0 & 0 & 0 & 0 & 0 \\ .0001 & -.0003 & 1.0002 & 0 & 0 & 0 & 0 & 0 \\ 0 & 0 & 0 & 1.0000 & 0 & 0 & 0 & -.0006 \\ 0 & 0 & 0 & 0 & 1.0000 & 0 & 0 & 0 \\ 0 & 0 & 0 & 0 & 0 & 1.0000 & 0 & 0 \\ 0 & 0 & 0 & 0 & 0 & 0 & 1.0000 & 0 \\ 0 & 0 & 0 & -.0006 & 0 & 0 & 0 & 1.8892 \end{bmatrix}$$

$$R = diag(1.0000, 1.0007, 1.0000, 1.0000, 1.0000, 1.8892, 1.0000)$$

$$X = \begin{bmatrix} X_{11} & X_{12} \\ X_{21} & X_{22} \end{bmatrix}$$

where,

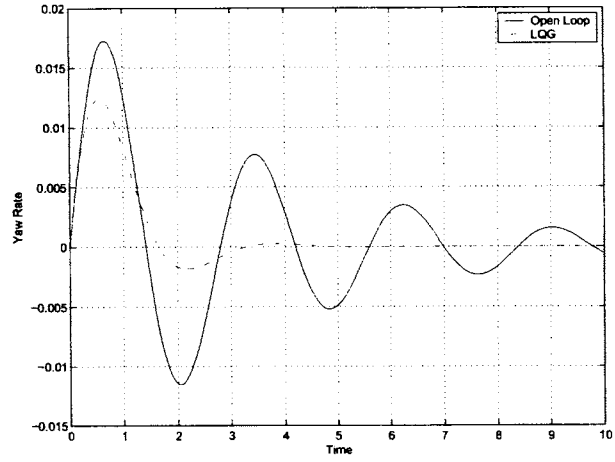

Figure 2.11 LQG yaw response

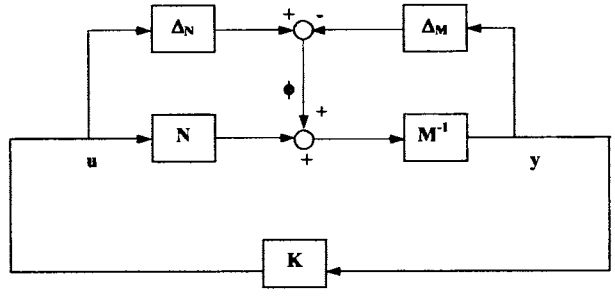

Figure 2.12 Feedback system for robustified design

$$X_{11} = \begin{bmatrix} 0.000 & 0.000 & 0.001 & -0.001 & 0.000 & 0.000 & 0.000 & 0.000 \\ 0.000 & 0.000 & 0.016 & -0.011 & 0.000 & 0.000 & 0.000 & 0.000 \\ 0.001 & 0.016 & 2.066 & 0.483 & 0.000 & 0.000 & 0.000 & 0.000 \\ -0.001 & -0.011 & 0.483 & 10.044 & 0.000 & 0.000 & 0.000 & 0.000 \\ 0.000 & 0.000 & 0.000 & 0.000 & 0.000 & -0.002 & 0.000 & 0.002 \\ 0.000 & 0.000 & 0.000 & 0.000 & -0.002 & 0.610 & 0.001 & -0.235 \\ 0.000 & 0.000 & 0.000 & 0.000 & 0.000 & 0.001 & 0.015 & 0.020 \\ 0.000 & 0.000 & 0.000 & 0.000 & 0.002 & -0.235 & 0.020 & 1.230 \end{bmatrix}$$

$$X_{12} = \begin{bmatrix} 0.000 & 0.000 & 0.000 & -0.006 & 0.000 & 0.000 & 0.000 & 0.000 \\ 0.000 & 0.000 & 0.000 & -0.003 & 0.000 & 0.000 & 0.000 & 0.000 \\ -0.000 & 0.000 & -0.000 & -0.162 & 0.000 & 0.000 & 0.000 & 0.000 \\ -0.001 & 0.000 & 0.000 & -0.591 & 0.000 & 0.000 & 0.000 & 0.000 \\ 0.000 & 0.000 & 0.000 & 0.000 & 0.000 & 0.000 & 0.000 & 0.000 \\ 0.000 & 0.000 & 0.000 & 0.000 & 0.000 & -0.013 & 0.000 & 0.002 \\ 0.000 & 0.000 & 0.000 & 0.000 & 0.000 & 0.000 & -0.003 & -0.001 \\ 0.000 & 0.000 & 0.000 & 0.000 & 0.000 & 0.005 & -0.003 & -0.002 \end{bmatrix}$$

$$X_{21} = \begin{bmatrix} 0.000 & 0.000 & -0.000 & -0.001 & 0.000 & 0.000 & 0.000 & 0.000 \\ 0.000 & 0.000 & 0.000 & 0.000 & 0.000 & 0.000 & 0.000 & 0.000 \\ 0.000 & 0.000 & -0.000 & 0.000 & 0.000 & 0.000 & 0.000 & 0.000 \\ -0.006 & -0.003 & -0.162 & -0.591 & 0.000 & 0.000 & 0.000 & 0.000 \\ 0.000 & 0.000 & 0.000 & 0.000 & 0.000 & 0.000 & 0.000 & 0.000 \\ 0.000 & 0.000 & 0.000 & 0.000 & 0.000 & -0.013 & 0.000 & 0.005 \\ 0.000 & 0.000 & 0.000 & 0.000 & 0.000 & 0.000 & -0.003 & -0.003 \\ 0.000 & 0.000 & 0.000 & 0.000 & 0.000 & 0.002 & -0.001 & -0.002 \end{bmatrix}$$

$$X_{22} = \begin{bmatrix} 0.000 & 0.000 & 0.000 & 0.002 & 0.000 & 0.000 & 0.000 & 0.000 \\ 0.000 & 0.000 & 0.000 & 0.000 & 0.000 & 0.000 & 0.000 & 0.000 \\ 0.000 & 0.000 & 0.000 & 0.000 & 0.000 & 0.000 & 0.000 & 0.000 \\ 0.002 & 0.000 & 0.000 & 2.384 & 0.000 & 0.000 & 0.000 & 0.000 \\ 0.000 & 0.000 & 0.000 & 0.000 & 0.000 & 0.000 & 0.000 & 0.000 \\ 0.000 & 0.000 & 0.000 & 0.000 & 0.000 & 0.000 & -0.000 & -0.000 \\ 0.000 & 0.000 & 0.000 & 0.000 & 0.000 & -0.000 & 0.001 & 0.000 \\ 0.000 & 0.000 & 0.000 & 0.000 & 0.000 & -0.000 & 0.000 & 0.000 \end{bmatrix}$$

$$Z = 1e4 \cdot \begin{bmatrix} Z_{11} & Z_{12} \\ Z_{21} & Z_{22} \end{bmatrix}$$

where,

$$Z_{11} = \begin{bmatrix} 1.354 & -0.062 & 0.000 & -0.001 & 0.000 & 0.000 & 0.000 & 0.000 \\ -0.062 & 0.067 & 0.000 & 0.000 & 0.000 & 0.000 & 0.000 & 0.000 \\ 0.000 & 0.000 & 0.000 & 0.000 & 0.000 & 0.000 & 0.000 & 0.000 \\ -0.001 & 0.000 & 0.000 & 0.000 & 0.000 & 0.000 & 0.000 & 0.000 \\ 0.000 & 0.000 & 0.000 & 0.000 & 0.859 & -0.000 & 0.005 & 0.001 \\ 0.000 & 0.000 & 0.000 & 0.000 & -0.000 & 0.000 & 0.000 & 0.000 \\ 0.000 & 0.000 & 0.000 & 0.000 & 0.005 & 0.000 & 0.002 & 0.000 \\ 0.000 & 0.000 & 0.000 & 0.000 & 0.001 & 0.000 & 0.000 & 0.000 \end{bmatrix}$$

$$Z_{12} = \begin{bmatrix} 1.351 & -0.062 & 0.000 & -0.001 & 0.000 & 0.000 & 0.000 & 0.000 \\ -0.043 & 0.066 & 0.000 & 0.000 & 0.000 & 0.000 & 0.000 & 0.000 \\ 0.001 & 0.000 & 0.000 & 0.000 & 0.000 & 0.000 & 0.000 & 0.000 \\ -0.001 & 0.000 & 0.000 & 0.000 & 0.000 & 0.000 & 0.000 & 0.000 \\ 0.000 & 0.000 & 0.000 & 0.000 & 0.440 & -0.000 & 0.004 & 0.001 \\ 0.000 & 0.000 & 0.000 & 0.000 & 0.001 & 0.000 & 0.000 & 0.000 \\ 0.000 & 0.000 & 0.000 & 0.000 & -0.009 & 0.000 & 0.001 & 0.000 \\ 0.000 & 0.000 & 0.000 & 0.000 & -0.002 & 0.000 & 0.000 & 0.000 \end{bmatrix}$$

$$Z_{21} = \begin{bmatrix} 1.351 & 0.043 & 0.001 & -0.001 & 0.000 & 0.000 & 0.000 & 0.000 \\ -0.062 & 0.066 & 0.000 & 0.000 & 0.000 & 0.000 & 0.000 & 0.000 \\ 0.000 & 0.000 & 0.000 & 0.000 & 0.000 & 0.000 & 0.000 & 0.000 \\ -0.001 & 0.000 & 0.000 & 0.000 & 0.000 & 0.000 & 0.000 & 0.000 \\ 0.000 & 0.000 & 0.000 & 0.000 & 0.436 & 0.001 & -0.009 & -0.002 \\ 0.000 & 0.000 & 0.000 & 0.000 & -0.000 & 0.000 & 0.000 & 0.000 \\ 0.000 & 0.000 & 0.000 & 0.000 & 0.004 & 0.000 & 0.001 & 0.000 \\ 0.000 & 0.000 & 0.000 & 0.000 & 0.001 & 0.000 & 0.000 & 0.000 \end{bmatrix}$$

$$Z_{22} = \begin{bmatrix} 1.419 & -0.033 & 0.001 & -0.001 & 0.000 & 0.000 & 0.000 & 0.000 \\ -0.0325 & 0.153 & 0.001 & 0.000 & 0.000 & 0.000 & 0.000 & 0.000 \\ 0.001 & 0.001 & 0.000 & 0.000 & 0.000 & 0.000 & 0.000 & 0.000 \\ -0.001 & 0.000 & 0.000 & 0.000 & 0.000 & 0.000 & 0.000 & 0.000 \\ 0.000 & 0.000 & 0.000 & 0.000 & 1.537 & 0.000 & -0.009 & -0.002 \\ 0.000 & 0.000 & 0.000 & 0.000 & 0.000 & 0.000 & 0.000 & 0.000 \\ 0.000 & 0.000 & 0.000 & 0.000 & -0.009 & 0.000 & 0.001 & 0.000 \\ 0.000 & 0.000 & 0.000 & 0.000 & -0.002 & 0.000 & 0.000 & 0.000 \end{bmatrix}$$

$$F = \begin{bmatrix} F_{11} & F_{12} \end{bmatrix}$$

where,

$$F_{11} = \begin{bmatrix} 0.000 & 0.004 & 0.501 & 0.114 & 0.000 & 0.000 & 0.000 & 0.000 \\ 0.001 & 0.009 & 1.093 & 0.246 & 0.000 & 0.000 & 0.000 & 0.000 \\ -0.000 & -0.006 & -0.672 & -0.163 & 0.000 & 0.000 & 0.000 & 0.000 \\ 0.000 & 0.000 & 0.000 & 0.000 & 0.001 & -0.351 & -0.007 & 0.127 \\ 0.000 & 0.000 & 0.000 & 0.000 & 0.000 & 0.000 & 0.000 & 0.000 \\ 0.000 & 0.000 & 0.000 & 0.000 & -0.001 & 0.197 & -0.038 & -0.126 \\ 0.000 & 0.000 & 0.000 & 0.000 & -0.000 & -0.027 & -0.384 & -0.491 \\ 0.000 & 0.000 & 0.000 & 0.000 & 0.002 & 0.204 & -0.697 & -0.439 \end{bmatrix}$$

$$F_{12} = \begin{bmatrix} 0.000 & 0.000 & -0.001 & -0.040 & 0.000 & 0.000 & 0.000 & 0.000 \\ -0.000 & 0.000 & 0.002 & -0.086 & 0.000 & 0.000 & 0.000 & 0.000 \\ 0.000 & 0.000 & -0.001 & 0.052 & 0.000 & 0.000 & 0.000 & 0.000 \\ 0.000 & 0.000 & 0.000 & 0.000 & -0.000 & 0.008 & 0.001 & -0.001 \\ 0.000 & 0.000 & 0.000 & 0.000 & 0.000 & 0.000 & 0.000 & 0.000 \\ 0.000 & 0.000 & 0.000 & 0.000 & 0.000 & -0.006 & 0.007 & 0.004 \\ 0.000 & 0.000 & 0.000 & 0.000 & -0.001 & -0.011 & 0.068 & 0.032 \\ 0.000 & 0.000 & 0.000 & 0.000 & -0.002 & -0.087 & 0.292 & 0.101 \end{bmatrix}$$

$$L = \begin{bmatrix} L_{11} & L_{12} \\ L_{21} & L_{22} \end{bmatrix}$$

where,

$$L_{11} = \begin{bmatrix} -0.943 & 0.002 & 0.000 & -0.000 & 0.000 & 0.000 & 0.000 & 0.000 \\ 0.249 & -0.952 & 0.001 & -0.000 & 0.000 & 0.000 & 0.000 & 0.000 \\ 4.865 & 13.714 & -0.999 & 0.022 & 0.000 & 0.000 & 0.000 & 0.000 \\ -85.586 & 8.383 & 0.006 & -0.917 & 0.000 & 0.000 & 0.000 & 0.000 \\ 0.000 & 0.000 & 0.000 & 0.000 & -0.965 & -0.000 & 0.002 & 0.001 \\ 0.000 & 0.000 & 0.000 & 0.000 & -18.350 & -1.046 & -0.200 & -0.106 \\ 0.000 & 0.000 & 0.000 & 0.000 & 1.025 & 0.000 & -0.904 & 0.012 \\ 0.000 & 0.000 & 0.000 & 0.000 & 25.766 & 0.060 & 0.588 & -0.406 \end{bmatrix}$$

$$L_{12} = \begin{bmatrix} .167 & 0.002 & 0.000 & -0.000 & 0.000 & 0.000 & 0.000 & 0.000 \\ 0.353 & 0.151 & 0.001 & -0.000 & 0.000 & 0.000 & 0.000 & 0.000 \\ 16.165 & 13.802 & 0.104 & 0.011 & 0.000 & 0.000 & 0.000 & 0.000 \\ -82.517 & 8.374 & 0.006 & 0.183 & 0.000 & 0.000 & 0.000 & 0.000 \\ 0.000 & 0.000 & 0.000 & 0.000 & 0.004 & -0.000 & 0.001 & 0.001 \\ 0.000 & 0.000 & 0.000 & 0.000 & 4.151 & 0.048 & -0.165 & -0.106 \\ 0.000 & 0.000 & 0.000 & 0.000 & -0.900 & 0.009 & 0.162 & 0.012 \\ 0.000 & 0.000 & 0.000 & 0.000 & -23.320 & 0.071 & 0.395 & 0.696 \end{bmatrix}$$

$$L_{21} = \begin{bmatrix} -0.053 & 0.003 & 0.000 & 0.000 & 0.000 & 0.000 & 0.000 & 0.000 \\ 0.000 & 0.000 & 0.000 & 0.000 & 0.000 & 0.000 & 0.000 & 0.000 \\ -0.000 & -0.001 & 0.000 & 0.000 & 0.000 & 0.000 & 0.000 & 0.000 \\ -54.330 & 2.384 & -0.012 & 0.055 & 0.000 & 0.000 & 0.000 & 0.000 \\ 0.000 & 0.000 & 0.000 & 0.000 & 0.001 & 0.000 & 0.000 & 0.000 \\ 0.000 & 0.000 & 0.000 & 0.000 & 0.380 & -0.001 & 0.008 & 0.002 \\ 0.000 & 0.000 & 0.000 & 0.000 & -0.104 & 0.000 & -0.030 & -0.001 \\ 0.000 & 0.000 & 0.000 & 0.000 & -0.134 & 0.000 & -0.015 & -0.001 \end{bmatrix}$$

$$L_{22} = \begin{bmatrix} -1.156 & 0.003 & 0.000 & 0.000 & 0.000 & 0.000 & 0.000 & 0.000 \\ 0.000 & -1.103 & 0.000 & 0.000 & 0.000 & 0.000 & 0.000 & 0.000 \\ -0.001 & -0.001 & -1.103 & 0.000 & 0.000 & 0.000 & 0.000 & 0.000 \\ -54.850 & 2.353 & -0.012 & -1.047 & 0.000 & 0.000 & 0.000 & 0.000 \\ 0.000 & 0.000 & 0.000 & 0.000 & -1.097 & 0.000 & 0.000 & 0.000 \\ 0.000 & 0.000 & 0.000 & 0.000 & -0.098 & -1.104 & 0.006 & 0.002 \\ 0.000 & 0.000 & 0.000 & 0.000 & 0.089 & -0.001 & -1.126 & -0.001 \\ 0.000 & 0.000 & 0.000 & 0.000 & 0.056 & -0.000 & -0.012 & -1.104 \end{bmatrix}$$

$$\gamma = 1.4501$$

In the McFarlane-Glover controller design the γ value represents the amount of co-prime uncertainty the McFarlane-Glover controlled system can allow. In this case with $\gamma = 1.4501$ the system can allow 69% co-prime uncertainty. The resulting McFarlane-Glover controller is a eighth order dynamic system where the singular values of the McFarlane-Glover controller are shown in Fig. (2.13).

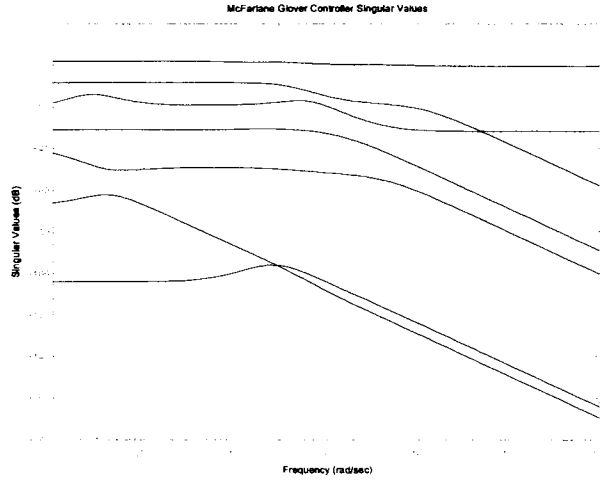

Figure 2.13 McFarlane-Glover controller singular values

The closed-loop eigenvalues are shown in Table (2.3).

Mode	Eigenvalue	Frequency (rad/s)	Damping ratio
Phugoid	$-0.020 \pm j0.027$	0.035	0.601
Short Period	$-3.460 \pm j3.392$	4.850	0.714
Spiral	-0.835	0.835	1.000
Roll Subsidence	-60.62	60.62	1.000
Dutch Roll	$-1.374 \pm j1.998$	2.430	0.567

Table 2.3 Closed-loop eigenvalues with McFarlane-Glover design

For McFarlane-Glover design, the open- and closed-loop initial condition responses for the angle of attack of, $\alpha = 0.0015$ rad and to an initial sideslip velocity disturbance of 6.5 ft/s are given in Figs. 2.14 through 2.20. The responses for the LQG controller design presented in section 3.1 are also included for comparison.

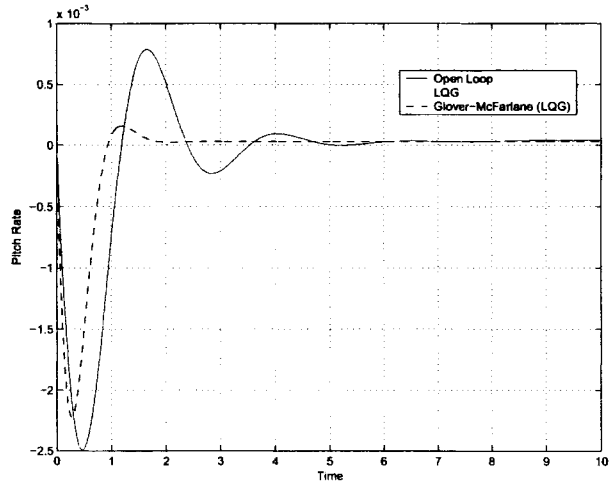

Figure 2.14 McFarlane-Glover pitch response

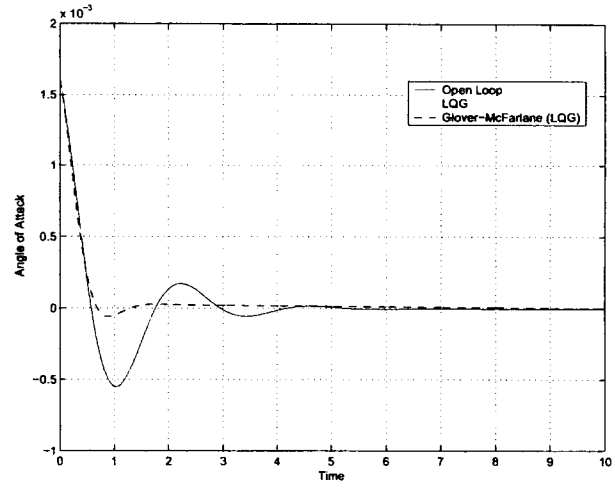

Figure 2.15 McFarlane-Glover angle of attack response

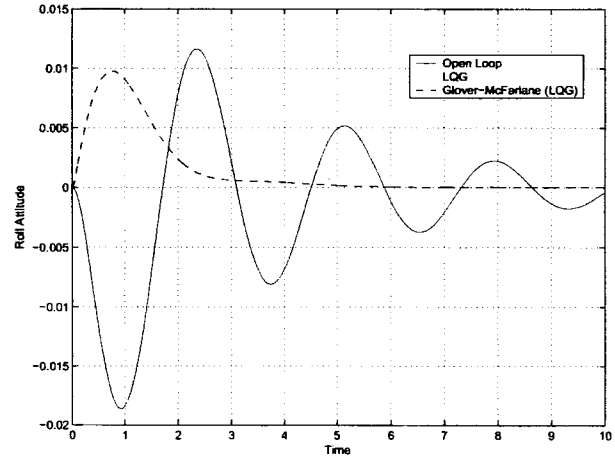

Figure 2.16 McFarlane-Glover roll attitude response

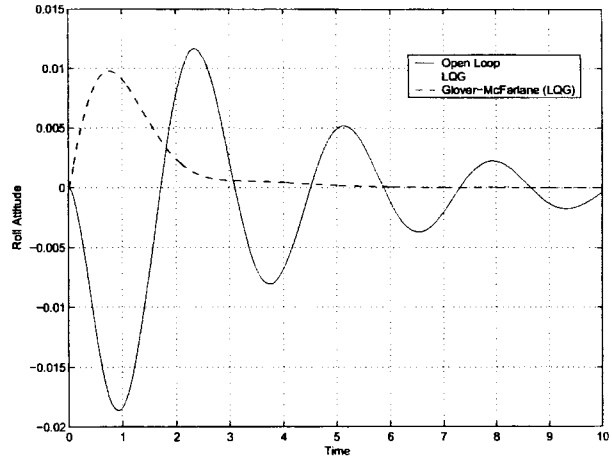

Figure 2.17 LQG roll response

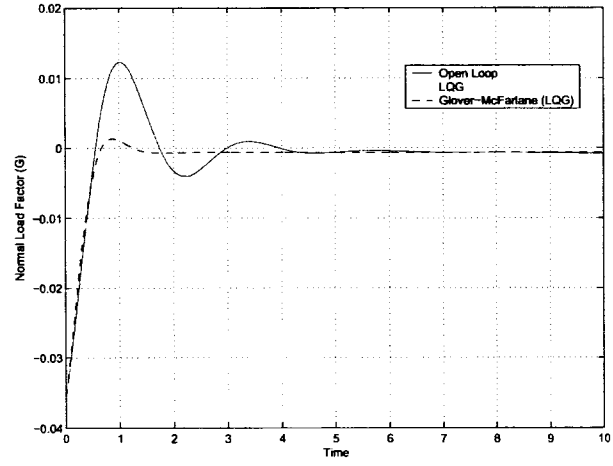

Figure 2.18 McFarlane-Glover normal load factor response

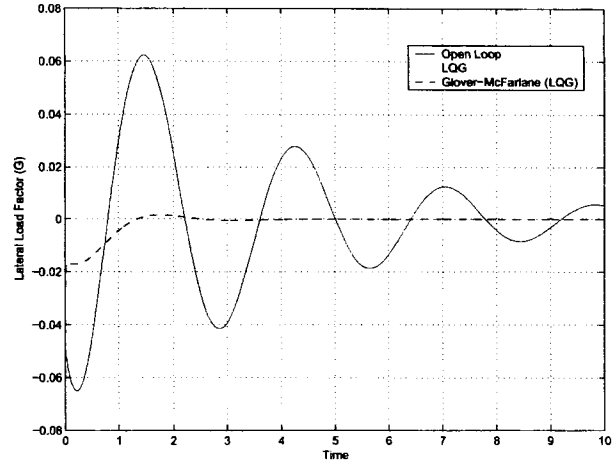

Figure 2.19 McFarlane-Glover lateral load response

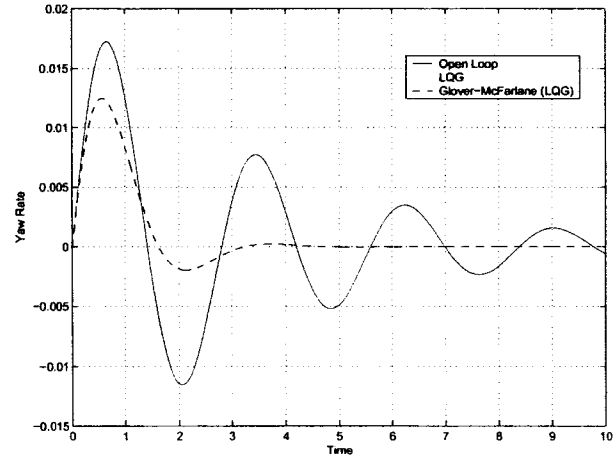

Figure 2.20 McFarlane-Glover yaw response

2.3.3 H_∞ Controller Design

In this section, an H_∞-based robust control design is presented for the fighter aircraft autopilot under consideration. Similar to the McFarlane-Glover design, the goal of H_∞ design is to shape the singular values of specified transfer functions over a given frequency range in order to meet the required performance and robustness properties.

To be able to draw a fair comparison between the H_∞ design and the McFarlane-Glover design a 20% uncertainty is assumed in both the damping ratio and the phugoid mode frequency for an H_∞ design. The relative difference between the set of uncertain plants and the nominal plant is shown in Fig. (2.21).

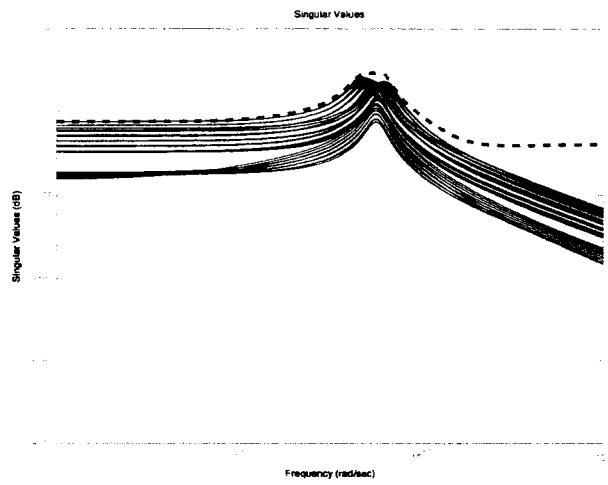

Figure 2.21 Relative uncertainty

The given additive uncertainty is bounded by a transfer function, $w_a(s)$, given by

$$w_a = \frac{0.1065s^4 + 0.02699s^3 + 0.00531s^2 + 0.0002985s + 4.408e-6}{s^4 + .02324s^3 + .006309s^2 + 7.144e-5s + 8.846e-6)} \tag{2.17}$$

This additive uncertainty description is then transformed into a multiplicative uncertainty description by taking the ratio of the additive uncertainty function to the maximum singular value of the nominal plant.

The multiplicative uncertainty weight, w_i, is then given by

$$w_i = \frac{0.612s^4 + 0.1474s^3 + 0.1752s^2 + 0.0015s + 1.0286e-5}{s^4 + 20.49s^3 + .8571s^2 + 0.08378s + .00158} \tag{2.18}$$

The closed-loop system can then be described as shown in Fig. (2.23) where the dotted box represents the actual uncertain plant. W_i is given as

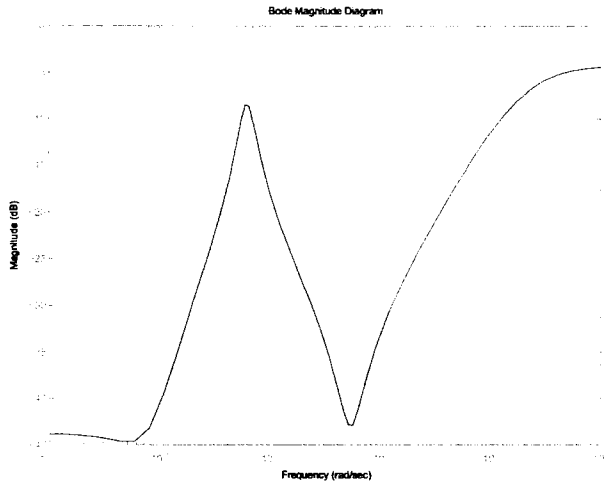

Figure 2.22 Multiplicative uncertainty weight

$$W_i = diag(w_i, w_i, w_i, w_i, w_i, w_i, w_i) \tag{2.19}$$

and the uncertainty matrix Δ_i satisfy the condition

$$\|\Delta_i\|_\infty \leq 1 \tag{2.20}$$

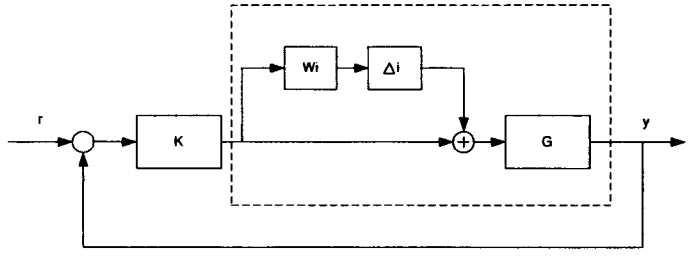

Figure 2.23 System with multiplicative uncertainty weight

The sensitivity function relates the reference disturbance input of the closed-loop system to the output of the plant and is given as

$$S = (I + GK)^{-1} \tag{2.21}$$

It is desired to attenuate the gain on the sensitivity function as much as possible in order limit the effects of the disturbance. In order to do so a weighting function, w_p, is used consisting of the form

$$w_p = \frac{(1\backslash M)s + w_b}{s + A} \tag{2.22}$$

where M is the bound on the sensitivity gain at high frequencies, w_b is the approximate bandwidth, and A is the bound at low frequencies. The weighting function, W_p, is chosen as a diagonal matrix consisting of the first order transfer functions w_ps and is given in Eq. (2.23).

$$W_p = diag(w_p, w_p, w_p, w_p, w_p, w_p, w_p) \tag{2.23}$$

w_ps in the above equation are given as described in Eq. (2.24). The specific $w_p(s)$ chosen is given below

$$w_p = \frac{0.18s + 1}{s + 4} \tag{2.24}$$

The bode plot of the weighting function is shown in Fig. (2.24).

The H_∞ controller is then determined by solving the stacked mixed sensitivity problem given as

$$\min_K \left\| \begin{matrix} w_p S \\ w_I T \end{matrix} \right\|_\infty < 1 \tag{2.25}$$

The block diagram of the generalized plant for the stacked problem is shown in Fig. (2.25)

The equations relating the inputs to the outputs are given as:

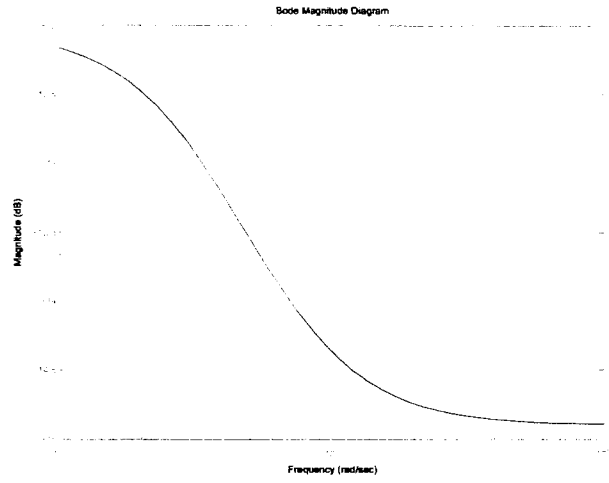

Figure 2.24 Sensitivity Weighting Function

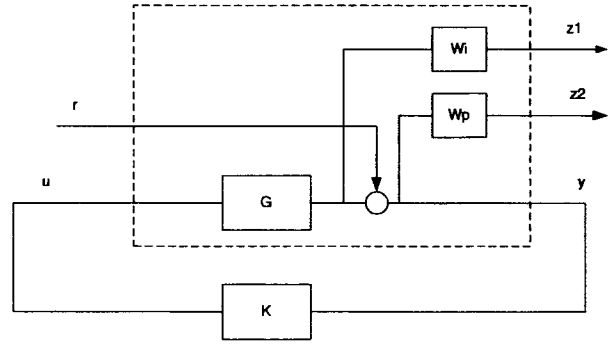

Figure 2.25 Generalized plant for the stacked problem

$$\begin{Bmatrix} z_1 \\ z_2 \\ y \end{Bmatrix} = \begin{bmatrix} 0 & w_I G \\ w_p & -w_p G \\ -1 & -G \end{bmatrix} \begin{Bmatrix} r \\ u \end{Bmatrix} \tag{2.26}$$

Using an H_∞ algorithm in the μ-toolbox of MATLAB, the controller was computed and the H_∞ norm function was determined to be 0.427. The controller obtained has 15 states with 7 inputs and 8 outputs with the corresponding singular value plot shown in Fig.(2.26).

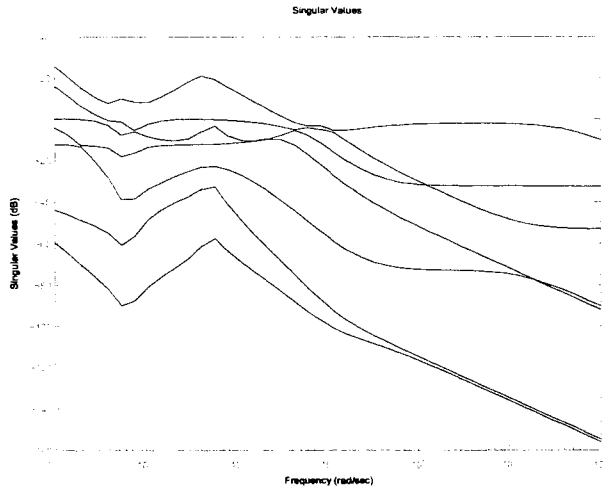

Figure 2.26 H_∞ Controller singular values

To show the robustness comparison the maximum sensitivity value plot of the H_∞ solution is shown in Fig. (2.35). The peak value shown is equal to 4.1.

The open-loop and closed-loop responses for the McFarlane-Glover controlled system to an initial angle of attack of, $\alpha = 0.0015$ rad and to an initial sideslip velocity disturbance of 6.5 ft/s are given in Figs. 2.27 through 2.33. The responses from the LQG controller presented in section 3.1 and the responses from the McFarlane-Glover controller presented in section 3.2 are also included for comparison.

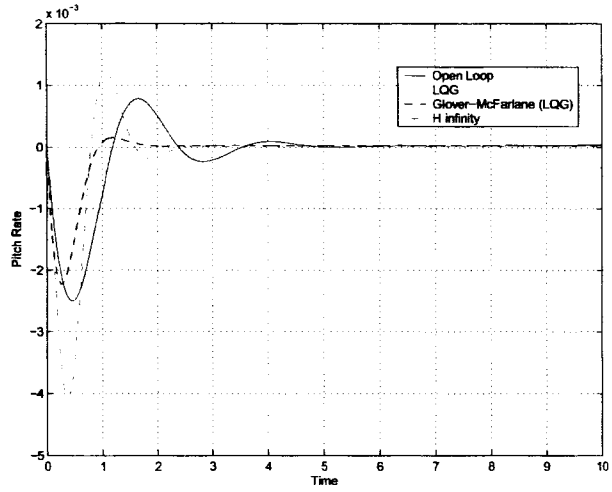

Figure 2.27 H_∞ pitch response

2.4 Comparison of Controller Designs

Figures 2.5-2.11 give a comparison of open- and closed-loop time responses for pitch, angle of attack, roll attitude, roll, normal load factor, lateral load factor, and yaw motion of the LQG controlled system. It can be seen that the baseline LQG design produces a very satisfactory response. However, LQG design assumes that the plant model is perfectly known which is often not the case, and therefore, the primary concern is that of robustness. The traditional LQG design methodology can not account for the plant uncertainties apriori which potentially can lead to closed-loop instabilities. Nevertheless, if one can tackle the problem of robustness separately LQG design is one of the most powerful techniques to design a controller.

For the case of the fighter aircraft under consideration, the McFarlane-Glover robustifying procedure was applied to the base-line LQG inner-loop design given in section 2.3.1. Figure (2.35) shows that the singular values of the sensitivity function for the LQG controlled system reach a peak value of 2.57. This high peak value indicates low stability margins that exist within the system at certain frequencies. The LQG closed-

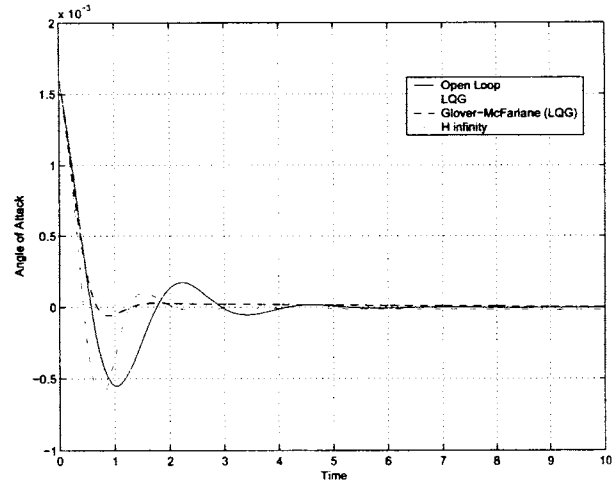

Figure 2.28 H_∞ angle of attack response

loop system is therefore post compensated using the robust stabilization technique of McFarlane and Glover. Using the left coprime factorization of the pre-compensated nominal plant, the perturbed plant can be written as in Eq. (2.11) where both Δ_M and Δ_N are unknown stable transfer functions which represent uncertainty in the system.

The objective of the robust stabilization given in section 2.3.2 is to minimize $\gamma \geq 1$ where γ is defined in Eq. (2.13). The value of γ_{min} obtained after robustification of the base-line LQG system was $\gamma = 1.4501$. This value indicates a significant improvement in the stability margins which can also be seen by observing the singular value plot in Fig. (2.35) where the peak of the maximum singular value of sensitivity function is reduced to 1.045. The comparison of the closed-loop time responses for baseline LQG design and robustified McFarlane-Glover design shown in Figs 2.14 through 2.20 shows that robustification is achieved without any noticeable degradation in performance. In addition, a quantitative measure of robustness is also obtained in the process.

For the H_∞ controller design the objective is to minimize the norm of the stacked cost function given in Eq. (2.26). Unlike the McFarlane-Glover problem the uncertainties in the system have to be modelled using weighting functions. As seen in the sensitivity plot

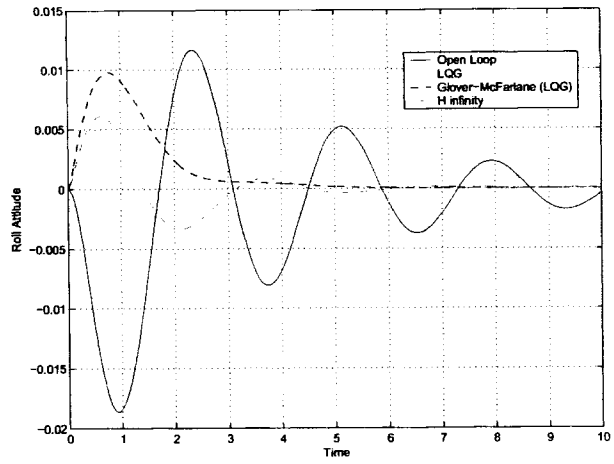

Figure 2.29 H_∞ roll attitude response

in Fig. (2.35) the H_∞ system peaks at 4.1 which is much higher than the LQG system or the McFarlane-Glover system. This is because the parametric uncertainty which was modelled is not handled well by the system and the controller can not allow for both low sensitivity and the modelled parametric uncertainty. It is also shown in Fig. 2.27 through 2.33 that the time response of the H_∞ system is worse than the responses from the LQG or the McFarlane-Glover systems.

2.5 Remarks

This chapter presented comparison of three different control designs for an autopilot of a fighter aircraft. The three designs considered included an LQG, McFarlane Glover robustifying design, and an H_∞ design. It was observed that the McFarlane Glover controller design was tolerant to a significant level of uncertainty while giving almost same level of performance as baseline LQG design. It was also observed that in comparison to H_∞ design the McFarlane-Glover design produced lower sensitivity peaks while maintaining a satisfactory level of performance in the closed-loop time response.

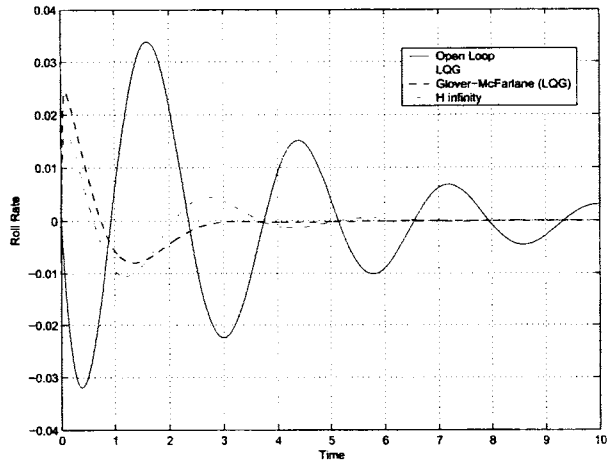

Figure 2.30 H_∞ roll response

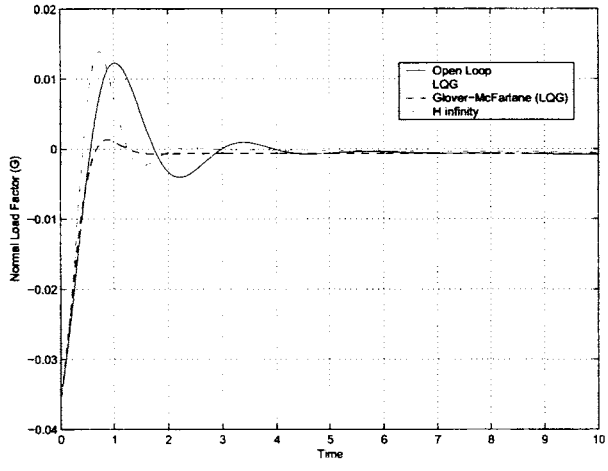

Figure 2.31 H_∞ normal load factor response

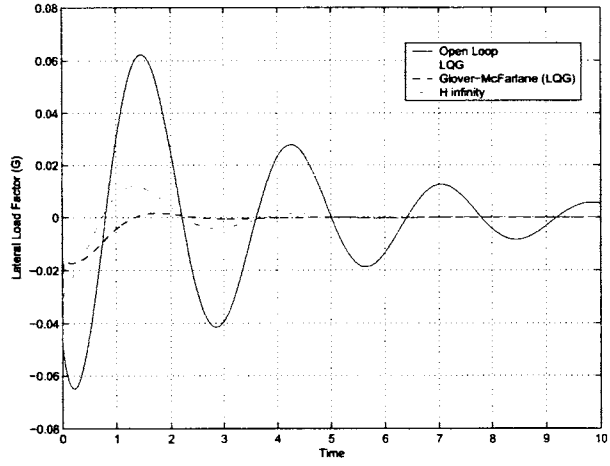

Figure 2.32 H_∞ lateral load response

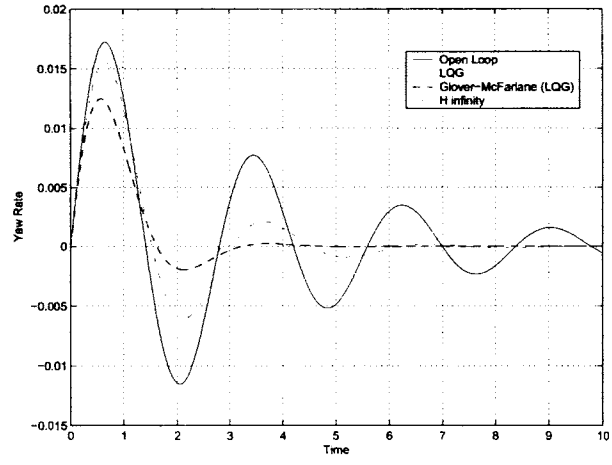

Figure 2.33 H_∞ yaw response

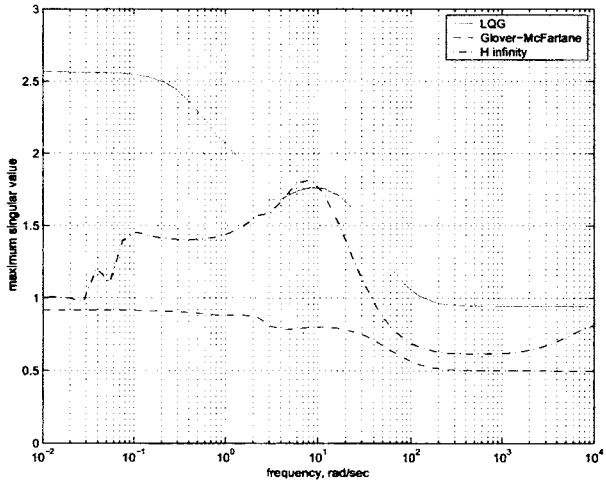

Figure 2.34 Maximum singular value of the closed-loop system

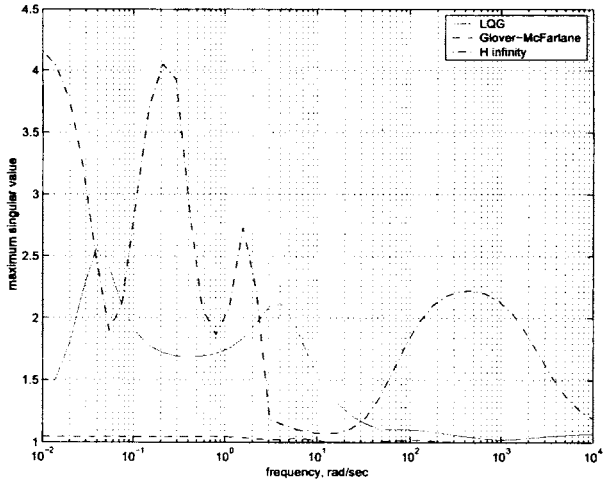

Figure 2.35 Maximum singular value of sensitivity function

3 AIRCRAFT FAULT DESCRIPTION

3.1 Introduction

Chapter 2 presented three different control design paradigms including two robust control methodologies which were aimed at increasing the robustness of the system in the presence of plant uncertainties and unwanted disturbances. The simulation results demonstrated the effectiveness of these designs in increasing the system's stability margins. However, these control systems which are designed to account for some level of plant uncertainty may not stabilize the aircraft in the presence of some kind of failure; for example, control surface (actuator) failure. The changes in the system dynamics caused by the failure of actuator and/or sensor could lead to weak, or sometimes, zero controllability and/or observability. The kind of uncertainties considered in the previous chapter dealt only with parametric inaccuracies and/or variations. One can conceivable argue that the dynamic changes that will take place as a result of failure can also be modelled as "uncertainty"; however, the magnitude of the changes will be significant enough to warrant a special design consideration at an early stage in the design. The reason being, one can only allow those failures in the system which will not destroy controllability of the system. In view of this, a thorough analysis of potential fault scenarios is needed prior to the design of controller. Moreover, the robust control design should explicitly account for failure modes under which controllability is not destroyed.

As stated previously, if the potential fault scenarios are not taken into account proactively during the control system design, the aircraft may not be able to survive a fault.

This chapter focuses on defining different failure scenarios for the aircraft model. This model will be used to demonstrate the fault-tolerant control design methodology in the next chapter. This chapter presents specific faults for the fighter aircraft model and also demonstrates the effect of these faults on the controller designed in the previous chapter which was based on parametric uncertainty considerations only.

3.2 Aircraft Model and Fault Description

A common control surface configuration for the most aircrafts is shown in Fig. (2.1). As mentioned previously, these control surfaces can be deflected to create forces to cause either longitudinal motion (Pitch and Lift) or lateral motion (Roll and Yaw). In order to gain an understanding of the purpose of each control surface, presented in table (3.1) is a list of various control surfaces and the resulting motion caused by the deflection of these control surfaces. Each of these control surfaces has the possibility of experiencing a

Control Surface	Symmetrical Deflection	Asymmetrical Deflection
Ailerons	N/A	Rolling Motion
Rudder	Yawing motion	N/A
" "	Takeoff / Landing Stability	N/A
Stabilator	Pitching Motion	Rolling Motion
Trailing Edge Flaps	Change in Lift Force	Aid in Rolling Motion
Leading Edge Flaps	Change in Lift Force	Aid in Rolling Motion
Speed Brake	Decrease Speed	N/A

Table 3.1 Response to control surface deflection

failure. The following is the list of possible failure conditions that can emerge due to one or many factors.

- Lock-In-Place (The control surface remains stationary in an unknown deflection due to a malfunction in the mechanical drive.)

- Hard-Over-Failure (The control surface is forced to the limit of its deflection due to a malfunction in the mechanical drive.)
- Float (The mechanical drive is disconnected from the control surface causing the control surface to deflect only by inertial forces.)
- Loss of Effectiveness (The aerodynamic force on the control surface is reduced to an ineffective magnitude due to damage to the control surface or to extreme flight conditions.)

3.2.1 Lock-In-Place Actuator Fault

The lock-in-place actuator failure [Mehra, Boskovic] is modelled as

$$u_j(t) = \bar{u}_j, \qquad t \geq t_j, j \in \{1, 2, ..., m\} \tag{3.1}$$

where $\bar{u}_j$ is a constant value corresponding to the locking position of the j_{th} actuator and t_j is the unknown failure time.

In the presence of lock-in-place actuator faults the input vector u to the plant (2.1) can be described as:

$$u(t) = \nu(t) + \sigma(\bar{u} - \nu(t)) \tag{3.2}$$

where $\nu(t)$ is the designed control input and

$$\bar{u}(t) = [\bar{u}_1, \bar{u}_2, ..., \bar{u}_m]^T \tag{3.3}$$

$$\sigma = diag\{\sigma_1, \sigma_2, ..., \sigma_m\} \tag{3.4}$$

where σ_i is given as

$$\sigma_i = \begin{cases} 1 & if\ the\ ith\ actuator\ fails,\ i.e.,\ u_j = \bar{u}_j \\ 0 & otherwise \end{cases} \tag{3.5}$$

3.3 Fault Model for Fighter Aircraft Configuration

The fault considered for the Fighter Aircraft model in Fig. (2.1) [REF] is that of a simultaneous lock-in-Place failure of both the rudder (u_7) and aileron (u_8) inputs. It is also assumed that these control surfaces lock in the neutral position (0^o deflection). The resulting input signal can be represented by

$$u(t) = \nu(t) + diag\{0,0,0,0,0,0,1,1\} \cdot (\bar{u} - \nu(t))$$

where ν(t) is defined as

$$\nu(t) = [\nu_1(t), \nu_2(t), \nu_3(t), \nu_4(t), \nu_5(t), \nu_6(t), \nu_7(t), \nu_8(t)]^T$$

and $\bar{u}$ due to the non-deflected locking positions of the rudder and ailerons is given as

$$\bar{u} = [0,0,0,0,0,0,0,0]^T$$

The input signal then becomes

$$u(t) = \begin{cases} [\nu_1(t), \nu_2(t), \nu_3(t), \nu_4(t), \nu_5(t), \nu_6(t), \nu_7(t), \nu_8(t)]^T & t < t_j \\ [\nu_1(t), \nu_2(t), \nu_3(t), \nu_4(t), \nu_5(t), \nu_6(t), 0, 0]^T & t \geq t_j \end{cases} \tag{3.6}$$

The fault in the rudder and aileron control surfaces is also equivalent to a change in the input matrix (B matrix) and the direct response matrix (D matrix) of the linearized system where the B matrix and the D matrix for the healthy system are

$$B_{healthy} = \begin{bmatrix} 0 & 0 & 0 & 0 & 0 & 0 & 0 & 0 \\ -.2 & -.645 & -.456 & 0 & 0 & 0 & 0 & 0 \\ -.241 & -.523 & .328 & 0 & 0 & 0 & 0 & 0 \\ 0 & 0 & 0 & 0 & 0 & 0 & 0 & 0 \\ 0 & 0 & 0 & -.21 & 0 & 0 & 0 & 30.37 \\ 0 & 0 & 0 & .574 & 0 & -.327 & .0044 & -.465 \\ 0 & 0 & 0 & .395 & 0 & 2.49 & 25.2 & 41.3 \\ 0 & 0 & 0 & 0 & 0 & 0 & 0 & 0 \end{bmatrix}$$

$$D_{healthy} = \begin{bmatrix} 0 & 0 & 0 & 0 & 0 & 0 & 0 & 0 \\ -.0062 & .021 & -.014 & 0 & 0 & 0 & 0 & 0 \\ 0 & 0 & 0 & 0 & 0 & 0 & 0 & 0 \\ 0 & 0 & 0 & 0 & 0 & 0 & 0 & 0 \\ 0 & 0 & 0 & 0 & 0 & 0 & 0 & 0 \\ 0 & 0 & 0 & -.00065 & 0 & 0 & 0 & .943 \\ 0 & 0 & 0 & 0 & 0 & 0 & 0 & 0 \end{bmatrix}$$

The B matrix for the system with the failed aileron and rudder can then be represented by

$$B_{failed} = B_{healthy} - B_{healthy} \cdot diag\{0,0,0,0,0,0,1,1\}$$

$$B_{failed} = \begin{bmatrix} 0 & 0 & 0 & 0 & 0 & 0 & 0 & 0 \\ -.2 & -.645 & -.456 & 0 & 0 & 0 & 0 & 0 \\ -.241 & -.523 & .328 & 0 & 0 & 0 & 0 & 0 \\ 0 & 0 & 0 & 0 & 0 & 0 & 0 & 0 \\ 0 & 0 & 0 & -.21 & 0 & 0 & 0 & 0 \\ 0 & 0 & 0 & .574 & 0 & -.327 & 0 & 0 \\ 0 & 0 & 0 & .395 & 0 & 2.49 & 0 & 0 \\ 0 & 0 & 0 & 0 & 0 & 0 & 0 & 0 \end{bmatrix}$$

and the corresponding D matrix is given as

$$D_{failed} = D_{healthy} - D_{healthy} \cdot diag\{0,0,0,0,0,0,1,1\}$$

$$D_{failed} = \begin{bmatrix} 0 & 0 & 0 & 0 & 0 & 0 & 0 & 0 \\ -.0062 & .021 & -.014 & 0 & 0 & 0 & 0 & 0 \\ 0 & 0 & 0 & 0 & 0 & 0 & 0 & 0 \\ 0 & 0 & 0 & 0 & 0 & 0 & 0 & 0 \\ 0 & 0 & 0 & 0 & 0 & 0 & 0 & 0 \\ 0 & 0 & 0 & -.00065 & 0 & 0 & 0 & 0 \\ 0 & 0 & 0 & 0 & 0 & 0 & 0 & 0 \end{bmatrix}$$

3.4 Effect on System Response

The baseline control system presented in (REF) is that of a linear quadratic regulator (LQR). It is known (Kalman, 1964; Safonov and Athens, 1977) that for LQR controlled systems (assuming that all states are available) the system will have infinite gain margin, a gain reduction margin equal to 0.5, and a minimum phase margin of 60°. The effects of actuator failure on the controlled aircraft, even with excellent stability margins, are given in Table (3.2). It lists the eigenvalues for the nominal (healthy plant) and the plant with the rudder and aileron failures. It is shown that the spiral mode becomes

Condition	Mode	Eigenvalue	Frequency (rad/s)	Damping ratio
Healthy		$-0.021 \pm j0.032$	0.039	0.55
Faulted	Phugoid	$-0.021 \pm j0.032$	0.039	0.55
Healthy		$-3.002 \pm j2.916$	4.190	0.717
Faulted	Short Period	$-3.002 \pm j2.916$	4.190	0.717
Healthy		-0.610	0.610	1.000
Faulted	Spiral	0.245	0.245	-1.000
Healthy		-36.230	36.230	1.000
Faulted	Roll Subsidence	-3.515	3.515	1.000
Healthy		$-1.176 \pm j1.931$	2.260	0.520
Faulted	Dutch Roll	$-1.301 \pm j2.528$	2.840	0.457

Table 3.2 LQR stability comparison

unstable after the ailerons and rudder failure occurs. This is due to the large dependence

of the motion of the aircraft on the rudder and aileron as seen from the large coefficients in the 7-th and 8-th columns of the B and D matrix. The closed-loop eigenvalues for the LQG controlled system are shown in Table (3.3), the robustified LQG closed-loop eigenvalues are shown in Table (3.4), and the H_∞ closed-loop eigenvalues are shown in Table (3.5).

Condition	Mode	Eigenvalue	Frequency (rad/s)	Damping ratio
Healthy		$-0.021 \pm j0.032$	0.039	0.550
Faulted	Phugoid	$-0.021 \pm j0.032$	0.039	0.550
Healthy		$-3.002 \pm j2.916$	4.190	0.717
Faulted	Short Period	$-3.002 \pm j2.916$	4.190	0.717
Healthy		-0.612	0.612	1.000
Faulted	Spiral	0.231	0.231	-1.000
Healthy		-36.230	36.230	1.000
Faulted	Roll Subsidence	$-3.590 \pm j0.265$	3.600	.997
Healthy		$-1.176 \pm j1.931$	2.260	0.520
Faulted	Dutch Roll	$-1.264 \pm j2.552$	2.850	0.444

Table 3.3 LQG stability comparison

Condition	Mode	Eigenvalue	Frequency (rad/s)	Damping ratio
Healthy		$-0.020 \pm j0.027$	0.035	0.601
Faulted	Phugoid	$-0.020 \pm j0.027$	0.035	0.601
Healthy		$-3.460 \pm j3.392$	4.850	0.714
Faulted	Short Period	$-3.460 \pm j3.392$	4.850	0.714
Healthy		-0.835	0.835	1.000
Faulted	Spiral	0.333	0.333	-1.000
Healthy		-60.62	60.62	1.000
Faulted	Roll Subsidence	$-3.571 \pm j0.168$	3.580	.999
Healthy		$-1.374 \pm j1.998$	2.430	0.567
Faulted	Dutch Roll	$-1.566 \pm j2.715$	3.130	0.500

Table 3.4 McFarlane Glover stability comparison

In order to demonstrate the effect of the aileron and rudder failure, the same initial state response that was used in Chapter 2 is simulated for both the nominal "healthy"

Condition	Mode	Eigenvalue	Frequency (rad/s)	Damping ratio
Healthy		$-0.020 \pm j0.033$	0.039	0.535
Faulted	Phugoid	$-0.021 \pm j0.033$	0.039	0.535
Healthy		$-2.370 \pm j3.420$	4.160	0.569
Faulted	Short Period	$-2.370 \pm j3.420$	4.850	0.714
Healthy		-0.806	0.806	1.000
Faulted	Spiral	0.104	0.104	-1.000
Healthy		-52.10	52.10	1.000
Faulted	Roll Subsidence	0.043	0.043	-1.000
Healthy		$-0.671 \pm j2.040$	2.150	0.313
Faulted	Dutch Roll	$0.037 \pm j0.671$	0.672	-0.052

Table 3.5 H_∞ stability comparison

system and the failed system. These responses are shown in Figs. (3.1-3.7)

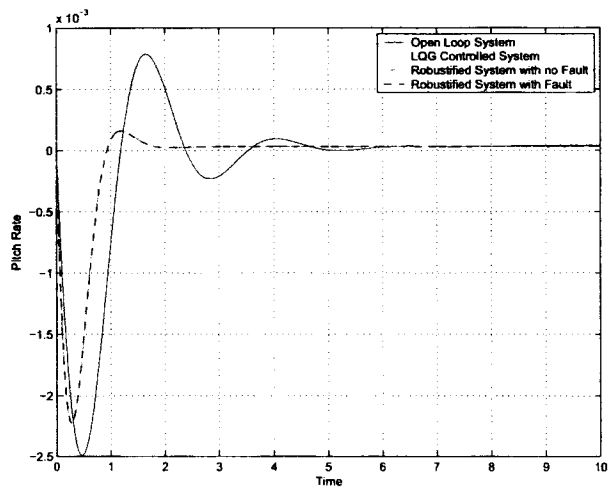

Figure 3.1 Failure comparison (pitch response)

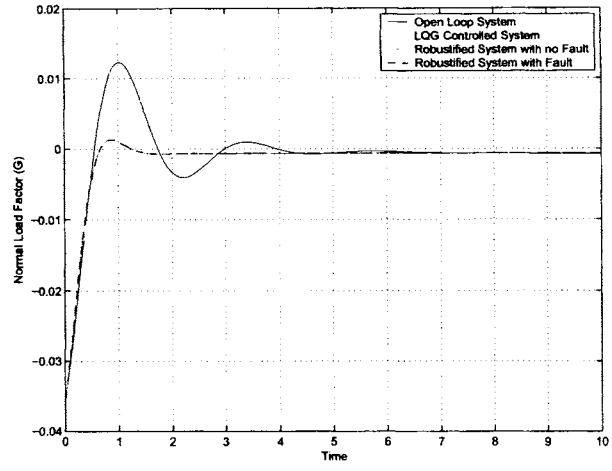

Figure 3.2 Failure comparison (normal load response)

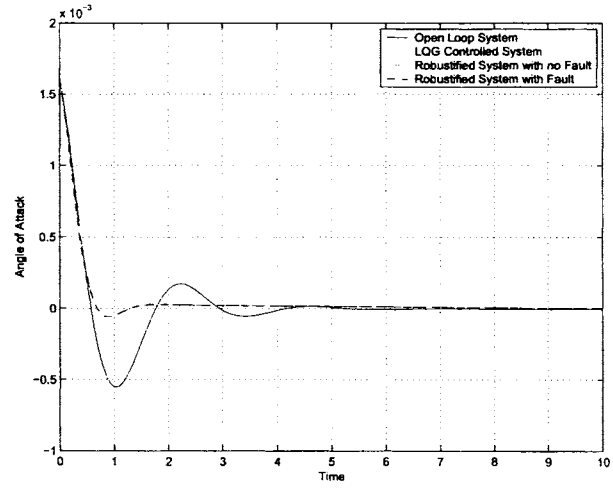

Figure 3.3 Failure comparison (angle of attack response)

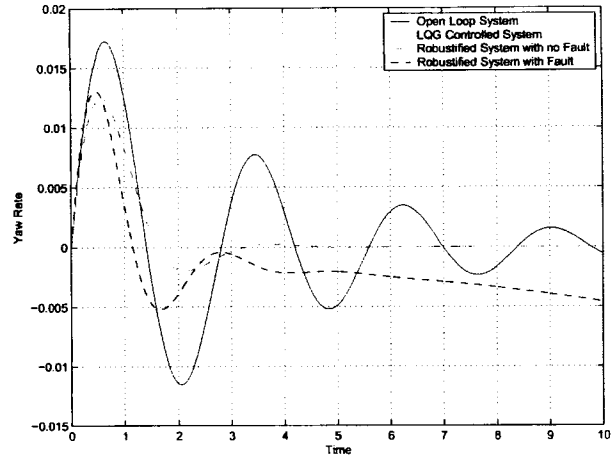

Figure 3.4 Failure comparison (yaw rate response)

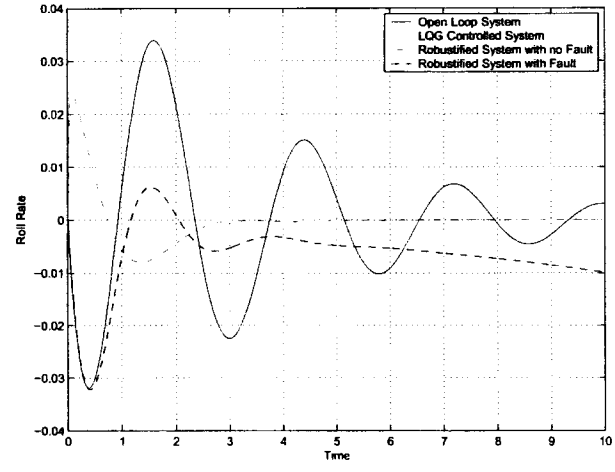

Figure 3.5 Failure comparison (roll rate response)

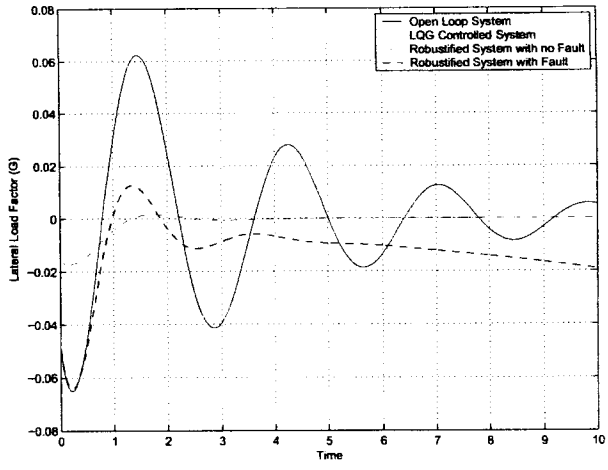

Figure 3.6 Failure comparison (lateral load response)

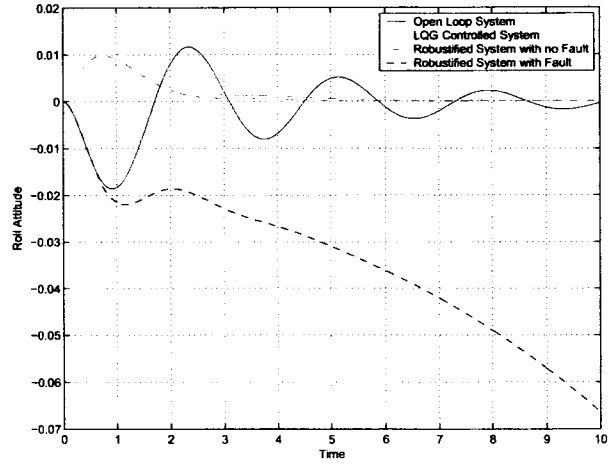

Figure 3.7 Failure comparison (roll attitude response)

3.5 Summary Remarks

This chapter presented failure scenarios for the aircraft model and its effect on the control system stability. In particular, the effect of lock-in-place actuator failure on the stability of the aircraft was analyzed. It was shown that the robust controller design

based on parametric uncertainty models could not survive the failure in the rudder and aileron control surfaces. Furthermore, in the case of the fighter aircraft, it is shown that only the lateral dynamics of the aircraft are affected by the fault. The reason for this is that the longitudinal and the lateral dynamics of the aircraft are completely decoupled as seen by the block diagonal structure of the state-space matrices and the only faults that occur are in the inputs to the lateral motion dynamics. The fact that longitudinal and lateral dynamics of the aircraft are decoupled indicates that there are only four possible control surface to create lateral motion. Since the rudder and aileron are assumed to fail the only control surfaces left to affect the lateral motion are the differential motion of the leading edge flaps and the differential motion of the trailing edge flaps.

4 FAULT TOLERANT CONTROLLER FORMULATION

This chapter is aimed at presenting various controller design methodologies that can systematically accommodate certain actuator failures at the design stage while maintaining a reasonable level of stability and performance in the autopilot design.

4.1 Introduction

The formulation of fault tolerant controller designs is presented and is demonstrated on the fighter aircraft model. Also, the method presented is compared to the results of an adaptive controller technique using a model of a Boeing 747's lateral dynamics. The controller design method is meant to form a controller which will keep the aircraft from destabilizing in the event of multiple actuator faults. The previous chapter demonstrated the effects of actuator faults on the closed-loop fighter aircraft system and results reflected that the robustified controller techniques of McFarlane and Glover and the parametric uncertainty-based H_∞ controller were not able to provide fault tolerance for the case of the rudder and aileron failures in the fighter aircraft because the designs were meant to account for only parametric uncertainty. In the case of failures such as loss or degradation of actuators the uncertainty model used in Chapter 2 (i.e., parametric type) can not capture these types of failures. Therefore, McFarlane-Glover type controller design can not be used as it does not allow to model a specific type of uncertainty such as actuator loss/degradation. H_∞ type controller design however is possible for such failures. As a result, this chapter focuses on the design of H_∞ fault-tolerant con-

troller for lock-in-place actuator failure. It is then shown that both the fighter aircraft model and the Boeing 747 model are able to be stabilized in the presence of multiple actuator faults.

4.2 Problem Formulation

The system considered for the controller formulation is a linear, time-invariant system as presented in Eq. (2.1) where A $\in \Re^{nxn}$, B $\in \Re^{nxm}$, C $\in$, $\Re^{rxn}$, and D $\in \Re^{rxm}$ are known constant parameter matrices. The performance output vector y(t) $\in \Re^r$ is known to be available for measurement and $u(t) = [u_1, ..., u_m]^T \in \Re^m$ is the input vector to the system. The fault considered is that of a lock-in-place actuator fault as modelled in Eq. (3.1), where the actuator failure times t_j are unknown. Furthermore, it is assumed that it is known which components of the input vector will fail. For the case of the fighter aircraft it is assumed that the rudder and ailerons are the only control surfaces capable of failure. The goal of the controller design is to ensure the system remains stable in the presence of the rudder and aileron actuator faults, specifically,

$$\Re(eig(G_{cl})) < 0 \qquad and \qquad \Re(eig(G_{clf})) < 0$$

where G_{cl} is the nominal "healthy" closed loop system and G_{clf} is the faulted closed loop system. In addition, the nominal closed loop system must present an acceptable level of time response performance and stability robustness.

4.3 Controller Formulation

The nominal closed loop plant is shown in block diagram form in Fig. (4.1) using the constant system matrices A, B, C, D

The system shown in Fig. (4.1) is equivalent to the system shown in Fig (4.2) where $y(t) = G \cdot u(t)$ and $G = C(sI - A)^{-1}B + D$ is the system's transfer function matrix.

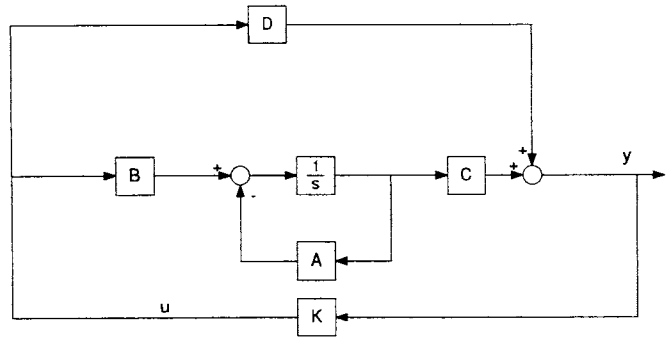

Figure 4.1 Nominal closed loop system

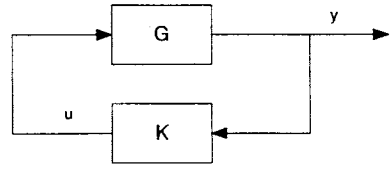

Figure 4.2 Standard block diagram form

The possibility of actuator failures in the system presents large uncertainties in the control input vector. To account for these uncertainties they must first be modelled mathematically; this is done in the controller formulation method presented here by introducing an additive uncertainty structure to both matrix B and matrix D. This is shown in Fig. (4.3) where the matrix uncertainty blocks $E_1 \in \Re^{nxm}$ and $E_2 \in \Re^{rxm}$ are defined below in Eq. (4.1) and Eq. (4.2).

$$E_1 = (B - Bf) \tag{4.1}$$

$$E_2 = (D - Df) \tag{4.2}$$

where

$$B_f = B - B \cdot \eta \tag{4.3}$$

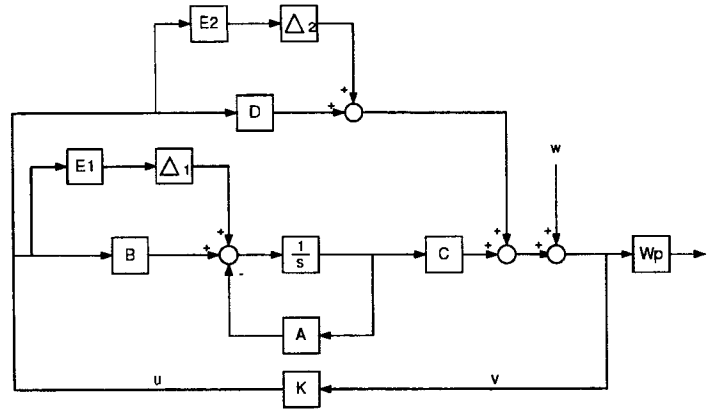

Figure 4.3 Closed loop system with failure Uncertainty

and

$$D_f = D - D \cdot \eta \tag{4.4}$$

η is a diagonal matrix to account for actuator failures and is described below in Eq. (4.5).

$$\eta = diag(\eta_1, \eta_2, ..., \eta_m) \tag{4.5}$$

where

$$\eta_i = \begin{cases} 1 & if\ the\ ith\ actuator\ is\ considered\ capable\ of\ failure \\ 0 & otherwise \end{cases} \tag{4.6}$$

$\Delta 1$ and $\Delta 2$ are defined as the delta blocks and by the H_∞ formulation method are given the condition

$$\|\Delta 1\|_\infty \leq 1 \qquad and \qquad \|\Delta 2\|_\infty \leq 1 \tag{4.7}$$

W_p is the weighting function on the performance output of the closed loop plant. The generalized plant "P", as shown in Fig. (4.4) is then formed.

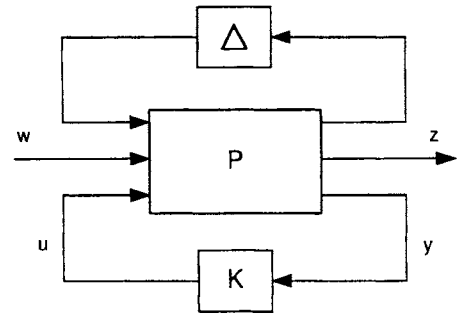

Figure 4.4 General plant configuration

where the system "P" can be defined as:

$$\begin{aligned} \dot{x}(t) &= A_1 x(t) + B_1 w(t) + B_2 u(t) \\ z(t) &= C_1 x(t) + D_{11} w(t) + D_{12} u(t) \\ y(t) &= C_2 x(t) + D_{21} w(t) + D_{22} u(t) \end{aligned} \tag{4.8}$$

The plant can then be partitioned into the transfer shown below in Eq. (4.9).

$$\begin{pmatrix} z(s) \\ y(s) \end{pmatrix} = \begin{pmatrix} P_{11}(s) & P_{12}(s) \\ P_{21}(s) & P_{22}(s) \end{pmatrix} \begin{pmatrix} w(s) \\ u(s) \end{pmatrix} \tag{4.9}$$

The closed loop transfer function from $w(s)$ to $z(s)$ is then given by the linear - fractional expression in Eq. (4.10).

$$F_L(P, K) \equiv P_{11} + P_{12} K (I - P_{22} K)^{-1} P_{21} \tag{4.10}$$

The goal of the H_∞ design is to then minimize $\|F_L(P, K)\|_\infty$ over all stabilizing LTI controllers. This can easily be done using different algorithms in MATLAB such as hinfsyn and hinflmi.

4.4 Simulation

The simulation presented here is that of a initial state response where the initial state vector is set as:

$$x_0 = [0, 1, 0, 0, 6.46, 0, 0, 0]^T$$

Using the method presented above the augmented system is formed, where the matrices E_1, E_2, and W_p are given below.

$$E_1 = \begin{bmatrix} 0 & 0 & 0 & 0 & 0 & 0 & 0 & 0 \\ 0 & 0 & 0 & 0 & 0 & 0 & 0 & 0 \\ 0 & 0 & 0 & 0 & 0 & 0 & 0 & 0 \\ 0 & 0 & 0 & 0 & 0 & 0 & 0 & 0 \\ 0 & 0 & 0 & 0 & 0 & 0 & 0.0044 & 30.370 \\ 0 & 0 & 0 & 0 & 0 & 0 & 25.20 & -0.4650 \\ 0 & 0 & 0 & 0 & 0 & 0 & 0 & 41.300 \\ 0 & 0 & 0 & 0 & 0 & 0 & 0 & 0 \end{bmatrix}$$

$$E_2 = \begin{bmatrix} 0 & 0 & 0 & 0 & 0 & 0 & 0 & 0 \\ 0 & 0 & 0 & 0 & 0 & 0 & 0 & 0 \\ 0 & 0 & 0 & 0 & 0 & 0 & 0 & 0 \\ 0 & 0 & 0 & 0 & 0 & 0 & 0 & 0 \\ 0 & 0 & 0 & 0 & 0 & 0 & 0 & 0 \\ 0 & 0 & 0 & 0 & 0 & 0 & 0 & 0.9430 \\ 0 & 0 & 0 & 0 & 0 & 0 & 0 & 0 \end{bmatrix}$$

$$W_p = diag(W_1, W_1, W_1, W_2, W_2, W_2, W_2)$$

where

$$W_1 = \frac{.7s + 20}{s + .1}$$

and

$$W_2 = \frac{.9s + 10}{s + .1}$$

The bode plot of W_p^{-1} is shown in Fig. (4.5).

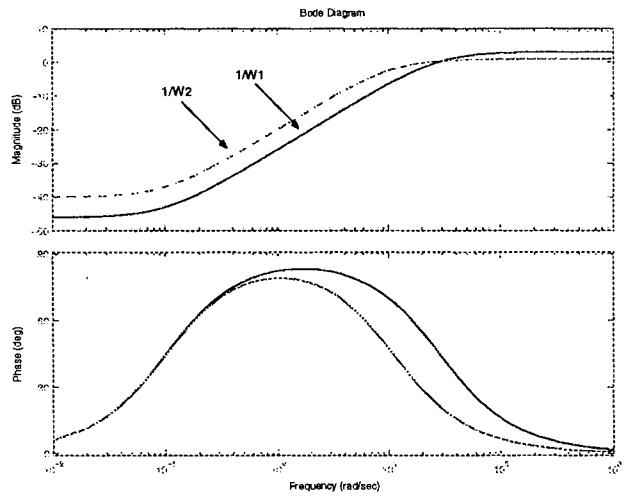

Figure 4.5 Performance weight bode plot

The augmented system is then given in Eq. (4.8) where the system matrices are calculated as:

$$A_1 = \begin{bmatrix} A & 0 \\ 4.464 \cdot C & -0.10 \cdot I_8 \end{bmatrix}$$

$$B_1 = \begin{bmatrix} E_1 \\ 3.148 \cdot E_2 \end{bmatrix}$$

$$B_2 = \begin{bmatrix} B \\ 4.464 \cdot D \end{bmatrix}$$

$$C_1 = \begin{bmatrix} 0_8 & 0_4 & 0_4 \\ 0_8 & 0_4 & 0_4 \\ .7 \cdot C & 4.464 \cdot I_4 & 0_4 \\ & 0_4 & 3.148 \cdot I_4 \end{bmatrix}$$

$$C_2 = \begin{bmatrix} C & 0_7 \end{bmatrix}$$

$$D_{11} = \begin{bmatrix} 0_8 \\ 0_8 \\ 0.90 \cdot E_2 \end{bmatrix}$$

$$D_{12} = \begin{bmatrix} I_8 \\ I_8 \\ 0.694 \cdot D \end{bmatrix}$$

$$D_{21} = \begin{bmatrix} E_2 \end{bmatrix}$$

$$D_{22} = \begin{bmatrix} D \end{bmatrix}$$

The resulting controller consists of 15 states, 7 inputs, and 8 outputs with the singular value plot shown in Fig. (4.6).

The sensitivity values for the healthy and faulted plant are shown below in Fig. (4.7).

As expected, this plot shows that the aircraft after the aileron and rudder fault has a much higher sensitivity to changes in the control loop. However, it is demonstrated in Figs. (4.8 - 4.14) that the aircraft after the aileron and rudder fault still maintains stability and adequate performance.

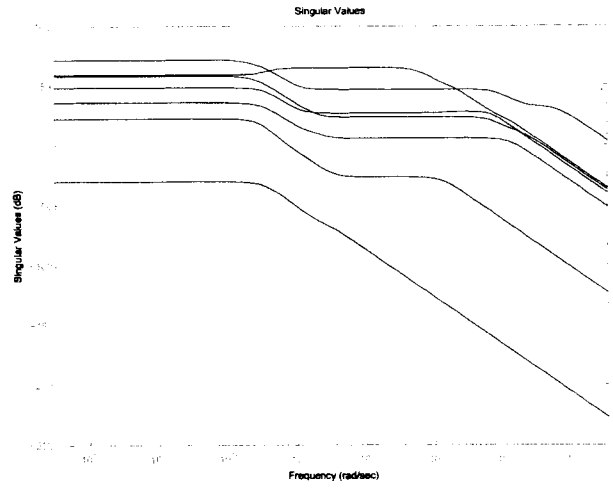

Figure 4.6 Controller singular values

4.5 Comparison of Robust H_∞ and Adaptive Methods

4.5.1 Mathematical model

The system used to compare the effectiveness of the robust H_∞ technique and the adaptive technique is a model of a Boeing 747 lateral dynamics. The aircraft is modelled as a linear time-invariant system with the state space form given as before in Eq. (2.1).

$$\begin{aligned} \dot{x}(t) &= Ax(t) + Bu(t) \\ y(t) &= Cx(t) + Du(t) \end{aligned}$$

where, the state variables are given by:

$$x = \begin{bmatrix} \beta & r & p & \phi \end{bmatrix}^T$$

The state variables represent side slip velocity (β), yaw rate (r), roll rate (p), and roll angle (ϕ) and the control inputs are given by

$$u = \begin{bmatrix} \delta_{r1} & \delta_{r2} & \delta_{r3} & \delta_{r4} \end{bmatrix}^T$$

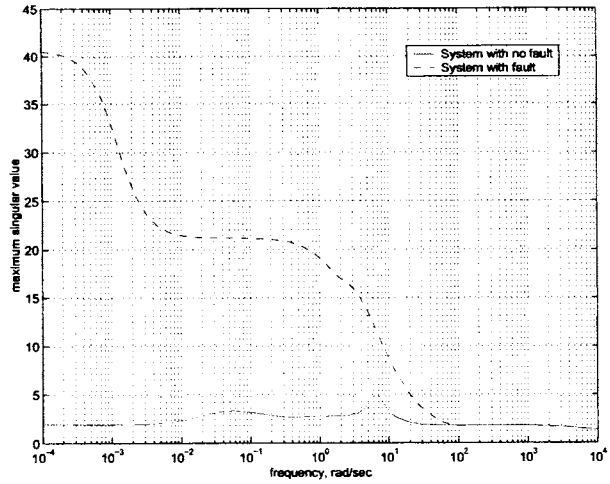

Figure 4.7 Maximum sensitivity singular values

where δ_{r1} through δ_{r4} are each inputs from different sections of a four section rudder. The system matrices A, B, C, and D (taken from [5]) at the flight condition of Mach 0.8 and an altitude of 40,000 ft are given by

$$A = \begin{bmatrix} -0.0558 & -0.9968 & 0.0802 & 0.0415 \\ 0.598 & -0.115 & -0.0318 & 0 \\ -3.05 & 0.388 & -0.465 & 0 \\ 0 & 0.0805 & 1 & 0 \end{bmatrix}$$

$$B = \begin{bmatrix} 0.0073 & 0.02 & 0.015 & 0.01 \\ -0.473 & -0.8 & -0.7 & -0.5 \\ 0.153 & 0.32 & 0.26 & 0.18 \\ 0 & 0 & 0 & 0 \end{bmatrix}$$

$$C = [I_4] \qquad D = [0_4]$$

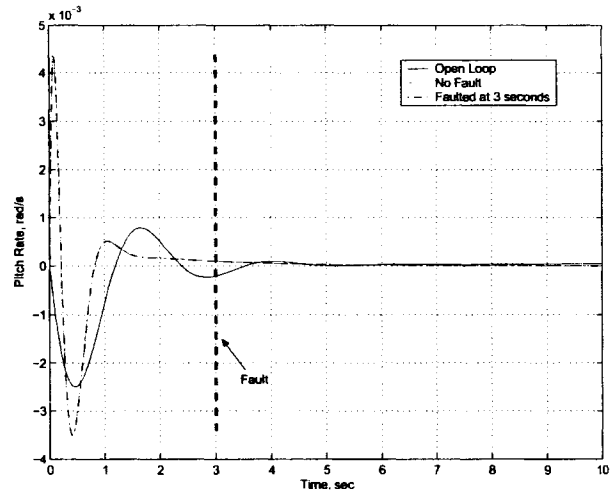

Figure 4.8 Pitch rate response (H_∞)

The eigenfrequencies of the open-loop system are given in Table 4.1.

Mode	Eigenvalue	Frequency (rad/s)	Damping ratio
Dutch Roll	$-0.033 \pm j0.947$	0.035	0.947
Spiral	-0.0073	0.0073	1.000
Roll Subsidence	-0.5627	.5627	1.000

Table 4.1 Eigenvalues of Boeing 747 lateral dynamics

4.5.2 Simulation

Using the method presented above the augmented system is formed, where the matrices E_1, E_2, and W_p are given below.

$$E1 = \begin{bmatrix} 0 & 0 & 0.015 & 0.01 \\ 0 & 0 & -0.7 & -0.5 \\ 0 & 0 & 0.26 & 0.18 \\ 0 & 0 & 0 & 0 \end{bmatrix}$$

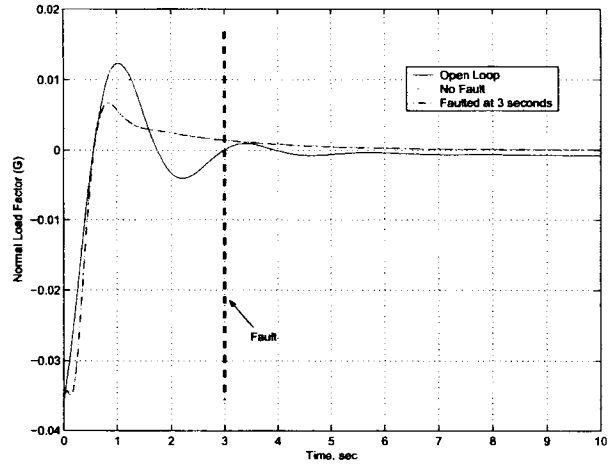

Figure 4.9 Normal load response (H_∞)

$$E2 = \begin{bmatrix} 0 & 0 & 0 & 0 \\ 0 & 0 & 0 & 0 \\ 0 & 0 & 0 & 0 \\ 0 & 0 & 0 & 0 \end{bmatrix}$$

$$W_p = diag(W_1, W_1, W_1, W_1)$$

where

$$W_1 = \frac{.5s + .9}{s + .2}$$

The bode plot of W_p^{-1} is shown in Fig. (4.15).

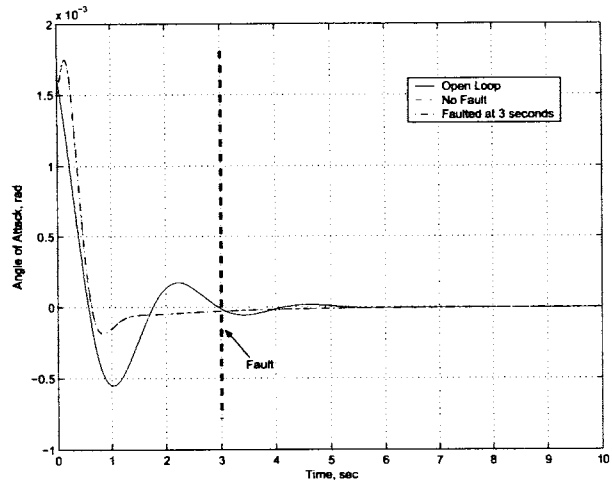

Figure 4.10 Angle of attack response (H_∞)

The augmented system is then given in Eq. (4.8) where the system matrices are calculated as:

$$A_1 = \begin{bmatrix} A & 0 \\ 0.8944 \cdot C & -0.20 \cdot I_4 \end{bmatrix}$$

$$B_1 = \begin{bmatrix} E_1 \\ 0_4 \end{bmatrix}$$

$$B_2 = \begin{bmatrix} B \\ 0_4 \end{bmatrix}$$

$$C_1 = \begin{bmatrix} 0_4 & 0_4 \\ 0.50 \cdot I_4 & 0.8944 \cdot I_4 \end{bmatrix}$$

$$C_2 = \begin{bmatrix} C & 0_4 \end{bmatrix}$$

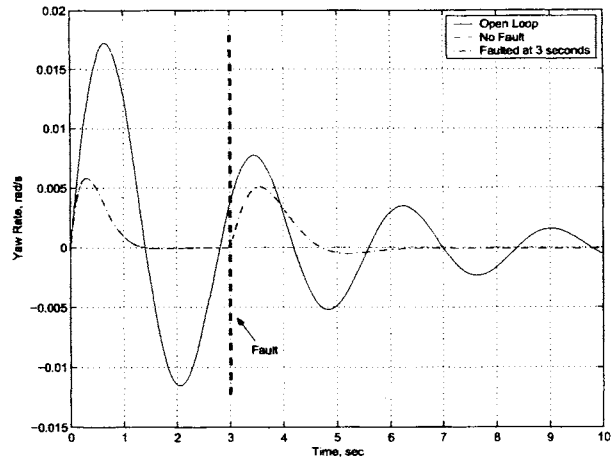

Figure 4.11 Yaw rate response (H_∞)

$$D_{11} = \begin{bmatrix} 0_4 \\ 0_4 \end{bmatrix}$$

$$D_{12} = \begin{bmatrix} I_4 \\ 0_4 \end{bmatrix}$$

$$D_{21} = \begin{bmatrix} 0_4 \end{bmatrix}$$

$$D_{22} = \begin{bmatrix} 0_4 \end{bmatrix}$$

The resulting controller consists of 8 states, 4 inputs, and 4 outputs with the singular value plot shown in Fig. (4.16).

The sensitivity values for the healthy and faulted plant are shown below in Fig. (4.17).

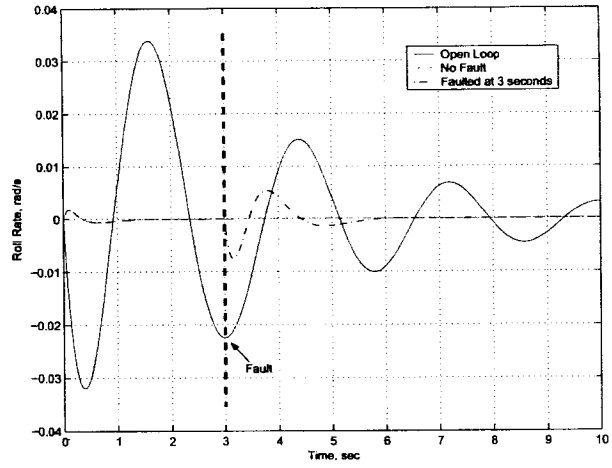

Figure 4.12 Roll rate response (H_∞)

As expected, this plot shows that the aircraft after the two rudder section faults has a much higher sensitivity to disturbances in the control loop. However, it is demonstrated in Figs. (4.18 - 4.21) that the aircraft after the faults still maintains stability and adequate performance.

4.5.3 Regulation

The goal of the regulator design is to force all desired signals to the smallest magnitude as possible for the complete operation period. The simulation presented here is that of a initial state response where the initial state vector is set as:

$$x_0 = [0.1, 0.01, -0.01, .5]^T$$

and the locking positions of the third and fourth rudder sections are set to $\bar{u}_3 = \bar{u}_4 = 0$ and the locking times are set to t_3 - t_4 =0. The time response of the state vector is demonstrated in Figs. (4.18 - 4.21) which shows that the system simulated with the fault does not degrade in performance at all compared with the healthy system.

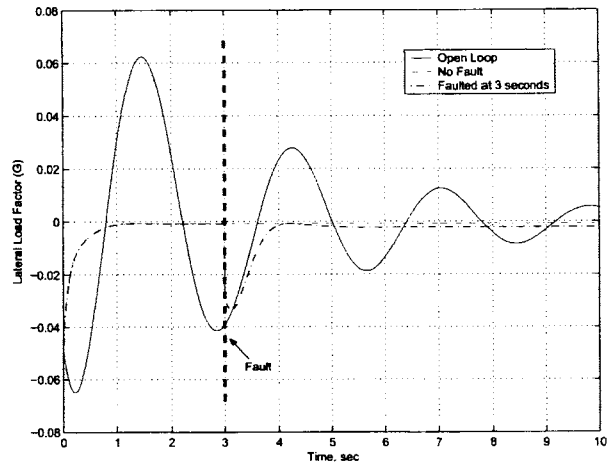

Figure 4.13 Lateral load response (H_∞)

4.5.4 Tracking

The goal of the tracking design is to "track" a given model or signal such that the error between the actual response and the model response is minimized. Adaptive control is used mainly with model tracking. The following simulation compares the results of both the H_∞ control technique presented in Section 2.3 and an adaptive control technique. In demonstrating these control techniques a reference model is used and is defined by the state space matrices $\{A_M, B_M, C_M, D_M\}$ (taken from [5]).

$$A_M = \begin{bmatrix} -0.0638 & -0.9744 & 0.0784 & 0.0406 \\ 0.9180 & -1.0120 & -0.407 & 0.0350 \\ -3.1780 & 0.7466 & -0.4939 & -0.0142 \\ 0 & 0.0805 & 1 & 0 \end{bmatrix}$$

$$B_M = \begin{bmatrix} 0.0075 & 0.005 \\ -0.4 & -0.3 \\ 0.14 & 0.1 \\ 0 & 0 \end{bmatrix}$$

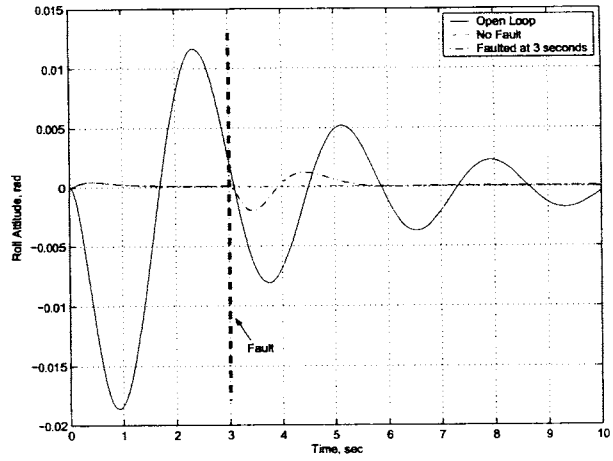

Figure 4.14 Roll attitude response (H_∞)

$$C_M = \begin{bmatrix} 1 & 0 & 0 & 0 \\ 0 & 1 & 0 & 0 \\ 0 & 0 & 1 & 0 \\ 0 & 0 & 0 & 1 \end{bmatrix}$$

$$D_M = \begin{bmatrix} 0 & 0 \\ 0 & 0 \\ 0 & 0 \\ 0 & 0 \end{bmatrix}$$

The reference inputs are given as $r_1(t) = .005sin(0.1t)$ rad, and $r_2(t) = .005rad$ and were taken from [5]. For the case of the Boeing 747 lateral motion control it is simulated that actuator u_4 fails at $t = 30s$ with $\bar{u}_4 = .15rad.$ and actuator u_3 fails at $t = 60s$ with $\bar{u}_3 = .1rad.$ The initial conditions are $x_0 = [0.1, 0.01, -0.01, .5]^T$ and $x_m(0) = [0, 0, 0, 0.6]^T$. The results are shown in Fig. (4.22 - 4.27). The response for the adaptive controller is only meant to show the similarities from the results in [5] and are

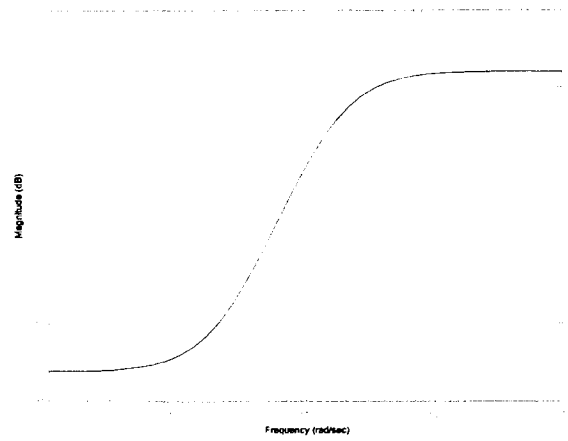

Figure 4.15 Performance weight bode plot

not meant to be the same response. As expected, the responses show adequate tracking throughout the duration of the simulation and the recovery time at the moments of the actuator faults is minimal.

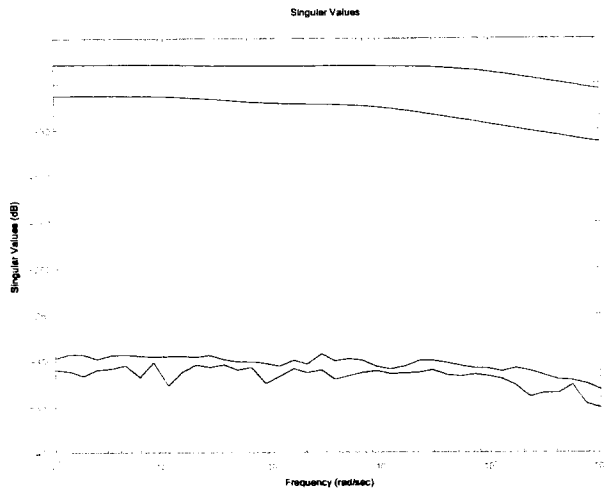

Figure 4.16 Controller singular values

4.6 Conclusions

This chapter presented a method to realize a reliable controller for a fighter aircraft with the considered failure scenario of a simultaneous aileron and rudder fault. Simulations of the closed loop system demonstrated that the reliable controller stabilized the faulted system while the robust controllers in Chapter 2 caused the faulted system to reach instability. It can be concluded from the simulations that fault tolerant control of an aircraft is possible with the use of a single time invariant reliable controller. The reliable control method was also compared to that of an adaptive control method through the simulation of a Boeing 747's lateral dynamics. The model tracking problem revealed that the reliable H_∞ controller created a higher closed loop tracking performance with less energy than that of the adaptive controller. An argument can then be made in that the reliable control method presented in this work is a better control choice given that the aircraft contains adequate open-loop stability and adequate redundancy in the control surfaces.

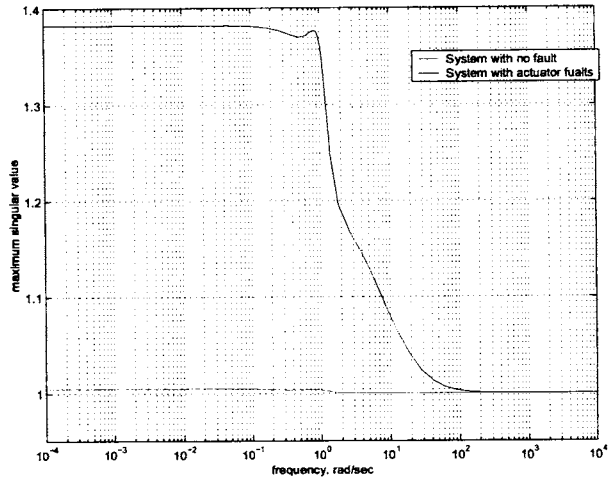

Figure 4.17 Maximum sensitivity singular values

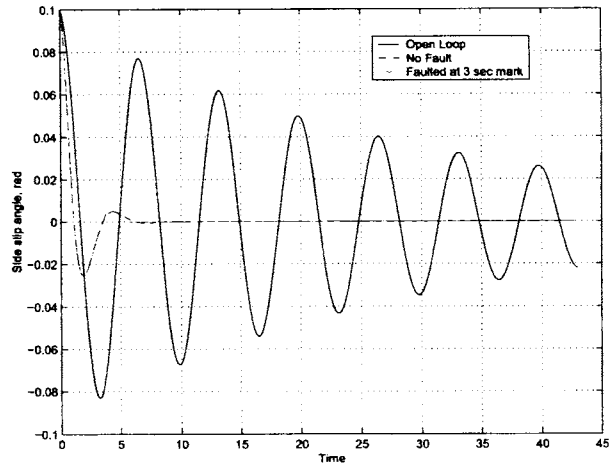

Figure 4.18 Side slip angle response

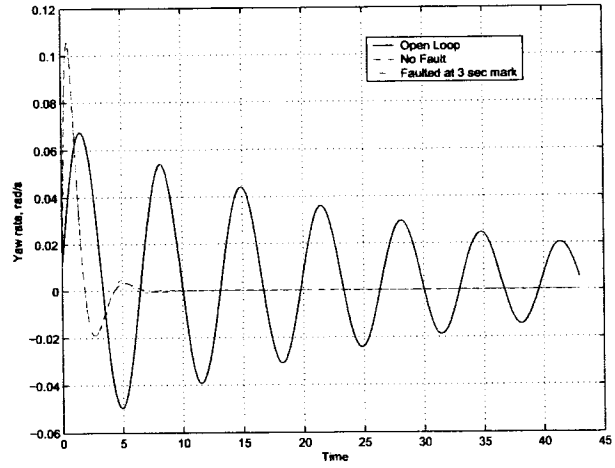

Figure 4.19 Yaw rate response

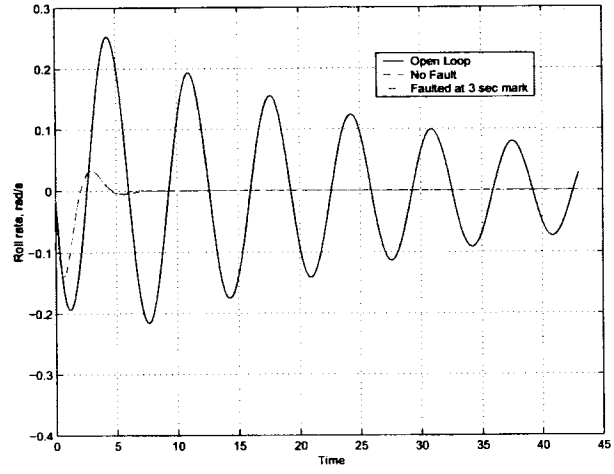

Figure 4.20 Roll rate response

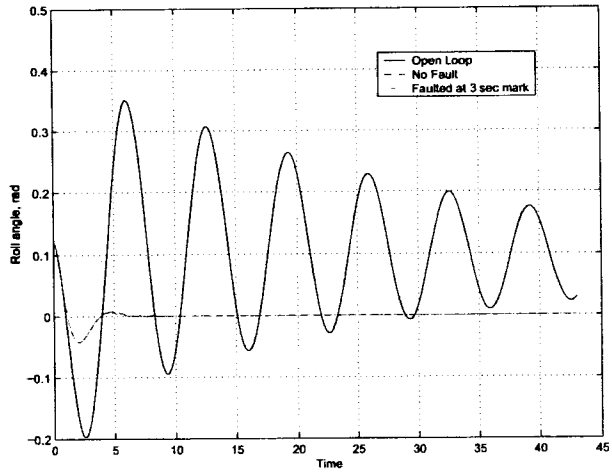

Figure 4.21 Roll angle response

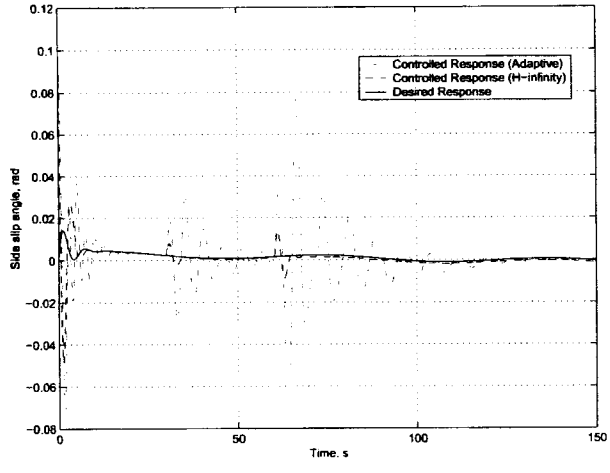

Figure 4.22 Side slip angle tacking response

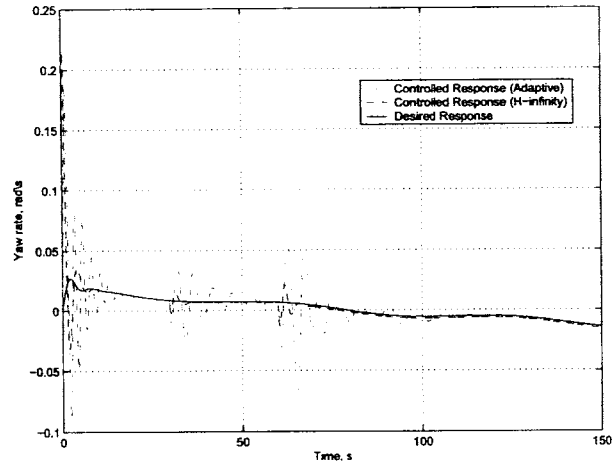

Figure 4.23 Yaw rate tracking response

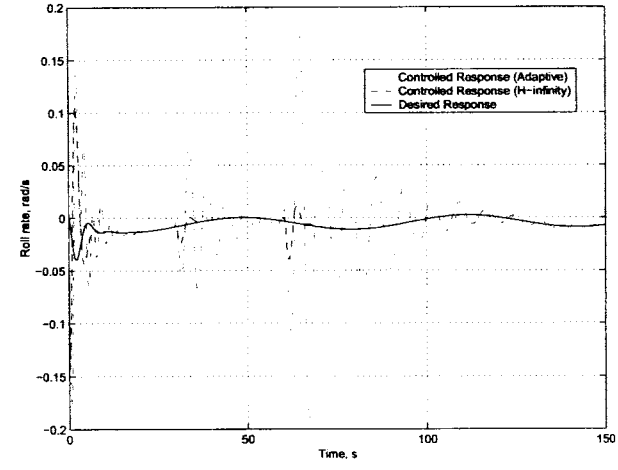

Figure 4.24 Roll rate tracking response

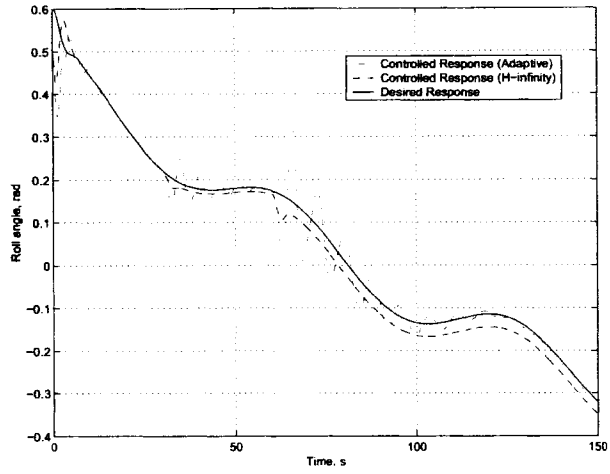

Figure 4.25 Roll angle tracking response

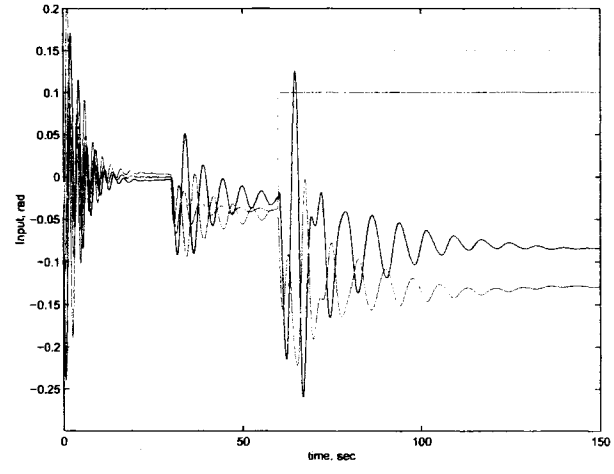

Figure 4.26 Adaptive controller inputs

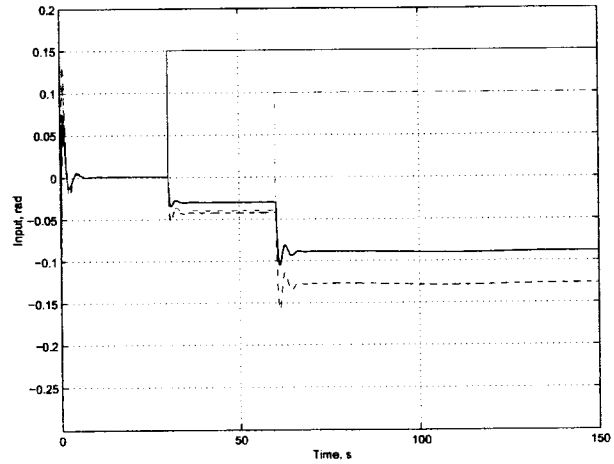

Figure 4.27 H_∞ controller inputs

5 CONCLUSIONS AND FUTURE WORK

In this chapter some concluding remarks and suggestions for future research are given. Suggestions for future research are by no means an exhaustive list.

5.1 Concluding Remarks

The research work presented in this thesis has two separate contributions to the field of flight control design. The first contribution is the analysis and synthesis of two advanced control design methodologies for design of an aircraft autopilot, in particular, the two methodologies that were evaluated included (1) McFarlane-Glover robustifying methodology and (2) the weighted sensitivity H_∞ design methodology. These control design methodologies were used to design an autopilot for the fighter aircraft model in Chapter 2 along with conventional LQG design. The methodologies presented enable the designer to account for uncertainties in the system in a systematic way. The uncertainties of interest are parametric uncertainties in specific modal parameters of the system. The McFarlane Glover controller accomplishes this by robustifying a pre-designed closed loop system which is designed solely for performance without regard to any stability robustness. The H_∞ method achieves uncertainty robustness by designing a controller to minimize weighted transfer functions where the weights are selected by the designer.

The two different controller design methodologies were demonstrated on a $8th$ order fighter aircraft model with both the lateral and longitudinal dynamics considered. The aircraft consisted of 7 measurable outputs and 8 controlled inputs. Results of the control

design methodologies demonstrate the large increase of robustness in the aircraft shown by the decrease in the sensitivity peaks.

Chapter 3 presented various actuator surface failure modes for the aircraft and their effects on the closed-loop performance of the aircraft. Using a simulation of a lock-in-place failure of the fighter aircraft's control surfaces (ailerons and rudder) it is shown in Chapter 3 that the aircraft equipped with traditional robust controller designs becomes largely unstable in the lateral dynamics. This is mainly due to the loss of the large input forces the rudder and ailerons provide to the control of the aircraft.

The second contribution of this thesis is the fault tolerant controller design methodology presented in Chapter 4. The results of the simulated fault on the aircraft system provide evidence that the robust controllers designed to account for only parametric uncertainty, such as those presented in Chapter 2, will not account for actuator faults in a aircraft. In order to account for such uncertainties a more specific controller formulation was developed using an additive uncertainty structure on the system matrices. The weighting scheme was developed to specifically account for the fault of both the ailerons and the rudder. The advantage of the method is that only a single controller is required to stabilize the aircraft and the need for a fault detection system is eliminated from the controller's perspective.

5.1.1 Suggestions for Future Work

The robust control design methodologies presented in this thesis uses a linearized model of the plant as the nominal design model. The control design methodologies presented in this thesis can take into account the uncertainties in the aircraft dynamics to some extent and use this linear model effectively as long as the flight conditions do not change by large amount. In the case of a big change in the flight conditions the designer has to obtain a new linearized model and repeat the design process. Future research needs to address how a designer can use multiple linearized models in different flight

regimes and associated uncertainty models effectively to synthesize a parameter-varying controller. The idea is to design a controller that maintains its structure throughout the flight envelope and only a selected few controller parameters change with the big changes in flight conditions.

Another area that needs to be explored is the merging of adaptive and the robust control design methodologies presented in this thesis to exploit their individual advantages. Future research should also investigate other fault-tolerant architectures based on model predictive control and compare them with the results of the work presented in this thesis. The design process presented here needs to be extended to account for various sensor failures as well. Eventually, the design methodology should be able to handle the failures in actuators and sensors simultaneously.

Finally, better methods for modelling actuator and sensor failures will be needed to design a less conservative and reliable controller.

BIBLIOGRAPHY

[1] Ashkenas, I. L., Magdaleno, R. E., and McRuer, D. T.: Flight Control and Analysis Methods for Studying Flying and Ride Qualities of Flexible Transport Aircraft. NASA CR 172201, August 1983.

[2] A.E.Bryson: *Control of Spacecraft and Aircraft* Princeton University Press, Princeton 1993.

[3] J. Burl, *Linear Optimal Control*, Addison-Wesley 1999.

[4] C.T. Chen,*Linear System Theory and Design*, Oxford University Press, New York 1999.

[5] Chen S., Tao G., and Joshi S.M.: Matching Conditions for Adaptive State Tracking Control of Systems With Actuator Failures, March 2002, vol.47.

[6] M. Corless; G. Leitmann, Bounded Controllers for robust exponetial convergence, Journal Optimization Theory Applications, vol. 76, no. 1, pp.1-12, 1993.

[7] B. Etkin, *Dynamics of Atmosphere Flight.* John Wiley and Sons, Inc., New York, 1972.

[8] H. Evers, J.R. Cloutier, C.F. Lin, W.R. Yuch and Q. Wang, Application of inegrated guidance and control schemes to a precision guided missile, Proc. American Control Conf, Chicago, IL, vol.4, pp. 3225-3230, 1992.

[9] B. Friedland, Control System Design: An introduction to State-Space Models. McGraw-Hill Book Company, New York, 1986.

[10] E.G. Gilbert and K.T. Tan, Linear systems with state and control constraints: the theory and applications of maximal output admissible sets, IEEE Transactions on Automatic Control, vol AC-36,pp. 1008-1020,1991.

[11] K. D. Hammet, W.C. Reigelsperger and S.S. Banda, High angle of attack short period flight control design with thrust vectoring, Proc. American Control Conf, Seattle, WA, vol. 1,pp. 170-174, 1995.

[12] V.Kudin and S. Lyashevskiy, Extending the solution of a class of problem of analytical design of nonlinear controllers, Automation and Remote Control, vol. 51,pt. 1,no. 7,pp. 880-888, 1990

[13] O. Leitmann, Guaranteed asymptotic stability for some linear systems with bounded uncertainties, ASME Journal of Dynamic Systems, Measurement, and Control, vol. 101,pp. 212-216, 1979.

[14] O. Leitmann, The Calculus of Variations and Optimal Control. Plenum Press, New york, 1981.

[15] X.Liii, A. Saberi and A. R. Teel, The almost disturbance decoupling problem with internal stability for linear systems.

[16] Y. Lin and E.D. Sontag, On control-Lyapanov functions under input constraints, Proc. Con. Decision and Control, Lake Buena Vista, Fl, vol. 1,pp. 640-645,1994.

[17] S. Lyashevskiy, Methods of Synthesis of Robust Regulators for Servomechansim and Stabilization Problems. The Academy of Sciences of the Ukraine Press, Kiev, 1991.

[18] S. Lyashevskiy, Robust nonlinear control of uncertain systems with state and control constraints, Proc. Conf. Decision and Control, New Orleans, LA, vol. 2,pp. 1670-1675, 1995.

[19] S. Lyashevskiy and A.U. Meyer, Control system analysis and design upon the Lyapunov method, Proc. American Control Conf., Seattle, WA, vol. 3, Pp. 3219-3224, 1995.

[20] B. Ma and W. S. Levine, "A new algorithm for solving optimal control problems with hard control constraints, end-point inequality constraints, and variable initial state," Proc. American Control Conf, Seattle, WA, vol. 2, pp. 2086-2092, 1995.

[21] C.I. Marnson and R.F. Stengel, Synthesis of robust control systems for a hypersonic aircraft, Proc. Conf Decision and Control, Lake Buena Vista, FL, vol. 4,pp. 3324-3329, 1994.

[22] McFarlane D. and Glover, K.: Robust Controller Design Using Normalized Coprime Factor Plant Descriptions, Vol. 138, Lecture Notes in Control and Information Sciences, Springer-Verlag, Berlin, 1990.

[23] McLean, D. and Aslam-Mir, S.: Reconfigurable Flight Control Systems, International Conference on Control, 25-28 Mar 1991, vol.1, Page(s): 234 -242.

[24] D. McRuer, I. Ashkenas and D.Graham, Aircraft Dynamics and Automation Control. Princeton University Press, Princeton, NJ, 1976.

[25] G.Meyer, L.R. Hunt and R.Su, "Nonlinear system guidance," Proc. Conf. Decision and Control, New Orleans, LA, vol.1,pp. 590-595,1995.

[26] R.C. Nelson, Flight Stability and Automatic Control. McGraw-Hill Book Company, New York, 1989.

[27] Newman, B., and Buttrill, C.: Conventional Flight Control for an Aeroelastic Relaxed Static Stability High-Speed Transport. Paper AIAA-95-3250-CP, Proc. AIAA GN&C Conference, Aug. 1995, Baltimore, MD, pp. 717-726.

[28] K. Ogata,*Modern Control Engineering*, Prentice Hall, New Jersey 1997.

[29] M. Pachter, P.R. Chandler and M. Meats, Reconfigurable tracking control with saturation, Proc. American Control Conf, Seattle, WA, vol. 3,pp. 3495-3499, 1995.

[30] S. Pandey, G. Leitmann and M. Corless, A deterministic controller for a new class of uncertain systems, Proc. Conf Decision and Control, Brighton, England, vol. 3,pp. 2615-2617,1991.

[31] I.R. Petersen and C.V. Hollot, A riccati equation approach to the stabilization of uncertain linear systems, Automatica, vol. 22,no. 4,pp. 397411, 1986.

[32] L.S. Pontryagun, V.O. Boltyanskiy, R.V. Gamkrelidze and B.F. Mishchenko, The Mathematical Theory of Optimal Processes. Interscience Publishers, Inc., New York, 1962.

[33] L. Rusnak, "Guidance law based on an exponential cost criterion for high order missile and maneuvering target," Proc. American Control Conf. Chicago, IL, vol. 3,pp. 2386-2390, 1992.

[34] A. Schumacher, "Rapid response missile ptch to trim flight control using sliding modes," Proc. Conf. Decision and Control, Lake Buena Vista, FL, vol. 4,pp. 3854-3859, 1994.

[35] D.D. Siljak, "Parameter space methods for robust control design: A guided tour," IEEE Transactions on Automatic Control, vol. AC-34,pp. 674-688, 1989.

[36] S. Skogestad; I. Postlethwaite,*Multivariable Feedback Control Analysis and Design*, John Wiley and Sons 1996.

[37] A.G. Sparks, L.M. Buffington and S.S. Banda, "Fighter aircratft lateral axis full envelope control law design," Proc. Conf Control Applications, Vancouver, Canada,pp. 21-26, 1993.

[38] J. Speyer and B.Z. Crues, "Approximate optimal atmospheric guidance law for aeroassisted plane-change maneuvers," Journal of Guidance, Control, wid Dynamics, vol. 13, no. 5,pp. 792-802, 1990.

[39] F. Tyan, and D.S. Bernstein, "Antiwindup conpensator synthesis for systems with saturating actuators," Proc. Conf Decision and Control, Lake Buena Vista, FL, vol. 1,pp. 150-155, 1994.

[40] C.L. Wan and D.S. Bernstein, "Nonlinear feedback control with global stabilization," Dynamics and Control, vol. 5, no. 4,pp. 321-346, 1995.

[41] K.A. Wise, "Applied control research topics in the aerospace industry," Proc. Conf Decision and Control, New Orleans, LA, vol. 1,pp. 751-756, 1995.

[42] K.A. Wise, "Comparison of six robustness tests evaluating missile autopilot robustness to uncertain aerodynamics," Journal of Guidance, Control, and Dynamics, vol. 15, no. 4,pp. 861-870, 1992.

[43] Yedavalli, R. K.: Flight Control Application of New Stability Robustness Bounds for Linear Uncertain Systems. *J. Guidance, Control, and Dynamics*, Vol. 16, No. 6, Nov.-Dec. 1993, pp.1032-1037.

[44] H.H. Yen, C.S. Hsu and S.S. Banda, "Fixed-order H infintiy compensator design," International Journal of Robust and Nonlinear Control, vol. 4, no. 3, Pp. 363-369, 1994.

[45] W.Yu, J.E. Piou and K.M. Sobel, "Robust eigenstructure assignment for the extended medium range air-to-air missile," Automatica, vol. 29, no. 4,pp. 889-898, 1993.